number of apoptotic cells on day 3. The number of engrafted MSCs in the MSC+AM group on day 14 was markedly higher than that in the MSC group. These results suggest that AM contributes to prolonging the viability of transplanted MSCs. In addition, AM inhibited apoptosis of non-MSCs, suggesting direct protective effects of AM on the ischemic penumbra. Furthermore, a combination of AM infusion and MSC transplantation markedly improved neurological functions compared with MSC transplantation or AM infusion alone. The infarct size on day 1 was smallest in the MSC+AM group, although infarct size on day 14 in the MSC+AM group tended to be small compared with that in other groups. Considering the angiogenic and antiapoptotic effects of AM and MSCs, administered AM may have additional or synergetic effects on MSC transplantation, leading to further improvement in neurological functions after stroke. Interestingly, a significant increase in body weight was observed in rats with low neurological score after treatment. A previous report has shown that body weight after stroke was higher in bFGF-treated rats than in vehicle-treated rats.[15] These results suggest that earlier recovery of neurological deficits might have restored impaired food intake after stroke.

MSC transplantation to treat brain ischemia has been investigated recently. We demonstrated previously the safety of AM infusion in patients with congestive heart failure.[16] Thus, combination therapy using AM infusion and MSC transplantation may be a novel and promising therapeutic strategy for treatment of stroke. However, systemically administered MSCs and AM may develop cancer and retinopathy via their angiogenic potential. Further studies are necessary to examine the safety and efficacy of this treatment.

In conclusion, AM enhanced the therapeutic potency of MSCs, including neurological improvement, possibly through inhibition of MSC apoptosis and induction of angiogenesis. A combination of AM infusion and MSC transplantation may be a new therapeutic strategy for treatment of stroke.

Acknowledgments

This work was supported by the Research Grant for Cardiovascular Disease (16C-6) from the Ministry of Health, Labour and Welfare; Industrial Technology Research Grant Program in 2003 from New Energy and Industrial Technology Development Organization of Japan; Health and Labor Sciences Research grants (H16-trans-008); and the Promotion of Fundamental Studies in Health Science of the Organization for Pharmaceutical Safety and Research of Japan.

References

1. Chen J, Li Y, Wang L, Zhang Z, Lu D, Lu M, Chopp M. Therapeutic benefit of intravenous administration of bone marrow stromal cells after cerebral ischemia in rats. *Stroke*. 2001;32:1005–1011.
2. Chen J, Zhang ZG, Li Y, Wang L, Xu YX, Gautam SC, Lu M, Zhu Z, Chopp M. Intravenous administration of human bone marrow stromal cells induces angiogenesis in the ischemic boundary zone after stroke in rats. *Circ Res*. 2003;92:692–699.
3. Chopp M, Li Y. Treatment of neural injury with marrow stromal cells. *Lancet Neurol*. 2002;1:92–100.
4. Mangi AA, Noiseux N, Kong D, He H, Rezvani M, Ingwall JS, Dzau VJ. Mesenchymal stem cells modified with Akt prevent remodeling and restore performance of infarcted hearts. *Nat Med*. 2003;9:1195–1201.
5. Kitamura K, Kangawa K, Kawamoto M, Ichiki Y, Nakamura S, Matsuo H, Eto T. Adrenomedullin: a novel hypotensive peptide isolated from human pheochromocytoma. *Biochem Biophys Res Commun*. 1993;192:553–560.
6. Tokunaga N, Nagaya N, Shirai M, Tanaka E, Ishibashi-Ueda H, Harada-Shiba M, Kanda M, Ito T, Shimizu W, Tabata Y, Uematsu M, Nishigami K, Sano S, Kangawa K, Mori H. Adrenomedullin gene transfer induces therapeutic angiogenesis in a rabbit model of chronic hind limb ischemia: benefits of a novel nonviral vector, gelatin. *Circulation*. 2004;109:526–531.
7. Kato H, Shichiri M, Marumo F, Hirata Y. Adrenomedullin as an autocrine/paracrine apoptosis survival factor for rat endothelial cells. *Endocrinology*. 1997;138:2615–2620.
8. Okumura H, Nagaya N, Itoh T, Okano I, Hino J, Mori K, Tsukamoto Y, Ishibashi-Ueda H, Miwa S, Tambara K, Toyokuni S, Yutani C, Kangawa K. Adrenomedullin infusion attenuates myocardial ischemia/reperfusion injury through the phosphatidylinositol 3-kinase/Akt-dependent pathway. *Circulation*. 2004;109:242–248.
9. Pittenger MF, Mackay AM, Beck SC, Jaiswal RK, Douglas R, Mosca JD, Moorman MA, Simonettii DW, Craig S, Marshak DR. Multilineage potential of adult human mesenchymal stem cell. *Science*. 1999;284:143–147.
10. Nagaya N, Fujii T, Iwase T, Ohgushi H, Itoh T, Uematsu M, Yamagishi M, Mori H, Kangawa K, Kitamura S. Intravenous administration of mesenchymal stem cells improves cardiac function in rats with acute myocardial infarction through angiogenesis and myogenesis. *Am J Physiol Heart Circ Physiol*. 2004;287:H2670–H2676.
11. Jean S, Haas P, Bauer P, Rolfs A, Wree A. Immunocytochemical characterization of in vitro PKH26-labelled and intracerebrally transplanted neonatal cells. *Acta Histochem*. 2000;102:273–280.
12. Sun Y, Jin K, Xie L, Childs J, Mao XO, Logvinova A, Greenberg DA. VEGF-induced neuroprotection, neurogenesis, and angiogenesis after focal cerebral ischemia. *J Clin Invest*. 2003;111:1843–1851.
13. Serrano J, Alonso D, Encinas JM, Lopez JC, Fernandez AP, Castro-Blanco S, Fernandez-Vizarra P, Richart A, Bentura ML, Santacana M, Uttenthal LO, Cuttitta F, Rodrigo J, Martinez A. Adrenomedullin expression is up-regulated by ischemia-reperfusion in the cerebral cortex of the adult rat. *Neuroscience*. 2002;109:717–731.
14. Watanabe K, Takayasu M, Noda A, Hara M, Takagi T, Suzuki Y, Yoshia J. Adrenomedullin reduces ischemic brain injury after transient middle cerebral artery occlusion in rats. *Acta Neurochir (Wien)*. 2001;143:1157–1161.
15. Jiang N, Finklestein SP, Do T, Caday CG, Charette M, Chopp M. Delayed intravenous administration of basic fibroblast growth factor (bFGF) reduces infarct volume in a model of focal cerebral ischemia/reperfusion in the rat. *J Neurol Sci*. 1996;139:173–179.
16. Nagaya N, Satoh T, Nishikimi T, Uematsu M, Furuichi S, Sakamaki F, Oya H, Kyotani S, Nakanishi N, Goto Y, Masuda Y, Miyatake K, Kangawa K. Hemodynamic, renal, and hormonal effects of adrenomedullin infusion in patients with congestive heart failure. *Circulation*. 2000;101:498–503.

Transplantation of Mesenchymal Stem Cells Improves Cardiac Function in a Rat Model of Dilated Cardiomyopathy

Noritoshi Nagaya, MD; Kenji Kangawa, PhD; Takefumi Itoh, MD; Takashi Iwase, MD; Shinsuke Murakami, MD; Yoshinori Miyahara, MD; Takafumi Fujii, MD; Masaaki Uematsu, MD; Hajime Ohgushi, MD; Masakazu Yamagishi, MD; Takeshi Tokudome, MD; Hidezo Mori, MD; Kunio Miyatake, MD; Soichiro Kitamura, MD

Background—Pluripotent mesenchymal stem cells (MSCs) differentiate into a variety of cells, including cardiomyocytes and vascular endothelial cells. However, little information is available about the therapeutic potency of MSC transplantation in cases of dilated cardiomyopathy (DCM), an important cause of heart failure.

Methods and Results—We investigated whether transplanted MSCs induce myogenesis and angiogenesis and improve cardiac function in a rat model of DCM. MSCs were isolated from bone marrow aspirates of isogenic adult rats and expanded ex vivo. Cultured MSCs secreted large amounts of the angiogenic, antiapoptotic, and mitogenic factors vascular endothelial growth factor, hepatocyte growth factor, adrenomedullin, and insulin-like growth factor-1. Five weeks after immunization, MSCs or vehicle was injected into the myocardium. Some engrafted MSCs were positive for the cardiac markers desmin, cardiac troponin T, and connexin-43, whereas others formed vascular structures and were positive for von Willebrand factor or smooth muscle actin. Compared with vehicle injection, MSC transplantation significantly increased capillary density and decreased the collagen volume fraction in the myocardium, resulting in decreased left ventricular end-diastolic pressure (11 ± 1 versus 16 ± 1 mm Hg, $P<0.05$) and increased left ventricular maximum dP/dt (6767 ± 323 versus 5138 ± 280 mm Hg/s, $P<0.05$).

Conclusions—MSC transplantation improved cardiac function in a rat model of DCM, possibly through induction of myogenesis and angiogenesis, as well as by inhibition of myocardial fibrosis. The beneficial effects of MSCs might be mediated not only by their differentiation into cardiomyocytes and vascular cells but also by their ability to supply large amounts of angiogenic, antiapoptotic, and mitogenic factors. (***Circulation.* 2005;112:1128-1135.**)

Key Words: myocytes ■ angiogenesis ■ heart failure ■ growth substances ■ transplantation

Despite advances in medical and surgical procedures, congestive heart failure remains a leading cause of cardiovascular morbidity and mortality.[1] Idiopathic dilated cardiomyopathy (DCM), a primary myocardial disease of unknown etiology characterized by a loss of cardiomyocytes and an increase in fibroblasts, is an important cause of heart failure.[2] Although myocyte mitosis and the presence of cardiac precursor cells in adult hearts have recently been reported,[3] the death of large numbers of cardiomyocytes results in the development of heart failure. Thus, restoring lost myocardium would be desirable for the treatment of DCM.

Mesenchymal stem cells (MSCs) are pluripotent, adult stem cells residing within the bone marrow microenvironment.[4] In contrast to their hematopoietic counterparts, MSCs are adherent and can be expanded in culture. MSCs can differentiate not only into osteoblasts, chondrocytes, neurons, and skeletal muscle cells but also into vascular endothelial cells[5] and cardiomyocytes.[6,7] In vitro, MSCs can be induced to differentiate into beating cardiomyocytes by 5-azacytidine treatment.[8] In vivo, MSCs directly injected into an infarcted heart have been shown to induce myocardial regeneration and improve cardiac function.[9] In addition, MSC implantation induces therapeutic angiogenesis in a rat model of hindlimb ischemia through vascular endothelial growth factor (VEGF) production by MSCs.[10,11] Myocardial blood flow abnormalities, even in the presence of angiographically normal coronary arteries, have been documented in patients with DCM.[12]

Received August 18, 2004; revision received April 28, 2005; accepted May 10, 2005.

From the Departments of Regenerative Medicine and Tissue Engineering (N.N., T.I., T.I., S.M.), Internal Medicine (N.N., M.Y., K.M.), Biochemistry (K.K., T.T.), and Cardiac Physiology (Y.M., T.F., H.M.), National Cardiovascular Center Research Institute, Osaka; the Cardiovascular Division (M.U.), Kansai Rosai Hospital, Hyogo; the Tissue Engineering Research Center (H.O.), National Institute of Advanced Industrial Science and Technology, Hyogo; and the Department of Cardiovascular Surgery (S.K.), National Cardiovascular Center, Osaka, Japan.

Reprint requests to Noritoshi Nagaya, MD, Department of Regenerative Medicine and Tissue Engineering, National Cardiovascular Center Research Institute, 5-7-1 Fujishirodai, Suita, Osaka 565-8565, Japan. E-mail nnagaya@ri.ncvc.go.jp

Circulation is available at http://www.circulationaha.org

DOI: 10.1161/CIRCULATIONAHA.104.500447

These findings raise the possibility that transplanted MSCs have beneficial effects on myocardial structure and function via myogenesis and angiogenesis. However, little information is available about the therapeutic potential of MSCs for DCM.

A unique model of myocarditis in the rat has been created by immunization with porcine cardiac myosin,[13] which results in severe heart failure characterized by increased cardiac fibrosis and left ventricular (LV) dilation.[14] Thus, the late phase of this model can serve as a model of DCM.

The purpose of this study was to investigate the following topics: (1) whether transplantation of MSCs induces myogenesis and angiogenesis, decreases collagen deposition in the myocardium, and thereby improves cardiac function in a rat model of DCM and (2) whether the beneficial effects of MSCs are mediated by their differentiation into cardiomyocytes and vascular cells and/or by their supplying angiogenic, antiapoptotic, and mitogenic factors.

Methods

Expansion of Bone Marrow MSCs

MSC expansion was performed according to previously described methods.[4] In brief, we humanely killed male Lewis rats and harvested bone marrow by flushing their femoral and tibial cavities with phosphate-buffered saline (PBS). Bone marrow cells were cultured in α-minimal essential medium supplemented with 10% fetal bovine serum and antibiotics. A small number of cells developed visible symmetric colonies by days 5 to 7. Nonadherent hematopoietic cells were removed, and the medium was replaced. The adherent, spindle-shaped MSC population expanded to $>5\times10^7$ cells within ≈4 to 5 passages after the cells were first plated.

Flow Cytometry

Cultured MSCs were analyzed by fluorescence-activated cell sorting (FACS) (FACScan flow cytometer, Becton Dickinson). Cells were incubated with fluorescein isothiocyanate (FITC)–conjugated mouse monoclonal antibodies against rat CD31 (clone TLD-3A12, Becton Dickinson), CD34 (clone ICO-115, Santa Cruz), CD45 (clone OX-1, Becton Dickinson), CD90 (clone OX-7, Becton Dickinson), vimentin (clone V9, Dako), and smooth muscle actin (SMA; clone 1A4, Dako). FITC-conjugated hamster anti-rat CD29 monoclonal antibody (clone Ha2/5, Becton Dickinson) and rabbit anti-rat c-Kit polyclonal antibody (clone C-19, Santa Cruz) were used. Isotype-identical antibodies served as controls.

Model of DCM

Male Lewis rats weighing 220 to 250 g (Japan SLC Inc, Hamamatsu, Japan) were used in this study. These isogenic rats served as donors and recipients of MSCs to simulate autologous implantation. DCM was produced by inducing experimental myocarditis, as described previously.[13,14] In brief, 1 mg (0.1 mL) of porcine heart myosin (Sigma) was mixed with an equal volume of Freund's complete adjuvant (Sigma) and injected into a footpad on days 1 and 7. Five weeks after immunization, these rats served as a model of heart failure due to DCM.

MSC Transplantation

In a preliminary experiment, we performed dose-response studies to obtain the maximal effects of cell transplantation. Because the effect of 10^6 MSCs was modest, we used 5×10^6 MSCs for transplantation. Five weeks after immunization, we injected a total of 5×10^6 MSCs/100 μL PBS, or PBS alone, into the myocardium at 10 points. In brief, the LV was divided into 3 levels (basal, middle, and apical). The basal and middle levels were each subdivided into 4 segments, and the apical level was subdivided into 2 segments. Injection into each segment was performed with a 27-gauge needle. Sham rats received intramyocardial injections of 100 μL PBS. This protocol resulted in the creation of 3 groups: DCM rats given MSCs (MSC-treated DCM group, n=10); DCM rats given PBS (untreated DCM group, n=10); and sham rats given PBS (sham group, n=10). The Animal Care Committee of the National Cardiovascular Center approved this experimental protocol.

Echocardiographic Studies

Echocardiographic studies were performed by an investigator, blinded to treatment allocation, at 5 weeks after immunization (before treatment) and 4 weeks after cell transplantation (after treatment). Two-dimensional, targeted M-mode tracings were obtained at the level of the papillary muscles with an echocardiographic system equipped with a 7.5-MHz transducer (HP Sonos 5500, Hewlett-Packard).[15] LV dimensions were measured according to the American Society for Echocardiology leading-edge method from at least 3 consecutive cardiac cycles. Fractional shortening was calculated as (LVDd−LVDs)/LVDd×100, where LVDd=LV diastolic dimension and LVDs=LV systolic dimension.

Hemodynamic Studies

Hemodynamic studies were performed 4 weeks after cell transplantation. A 1.5F micromanometer-tipped catheter (Millar Instruments) was inserted into the right carotid artery for measurement of mean arterial pressure.[16] Next, the catheter was advanced into the LV for measurement of LV pressure. Hemodynamic variables were measured with a pressure transducer (model P23 ID, Gould) connected to a polygraph. After completion of these measurements, the left and right ventricles were excised and weighed.

Histological Examination

To detect fibrosis in cardiac muscle, the LV myocardium (n=5 from each group) was fixed in 10% formalin, cut transversely, embedded in paraffin, and stained with Masson's trichrome. Transverse sections were randomly obtained from the 3 levels (basal, middle, and apical), and 20 randomly selected fields per section (n=60 per animal) were analyzed. After each field was scanned and computerized with a digital image analyzer (WinRoof, Mitani Co), collagen volume fraction was calculated as the sum of all areas containing connective tissue divided by the total area of the image.[15]

To detect capillaries in the myocardium, samples of harvested muscle (n=5 each) were embedded in OCT compound (Miles Scientific), snap-frozen in LN_2, cut into transverse sections, and stained for alkaline phosphatase by an indoxyltetrazolium method. Transverse sections were randomly obtained from the 3 levels (basal, middle, and apical), and 5 randomly selected fields per section (n=15 per animal) were analyzed. The number of capillaries was counted by light microscopy at a magnification of ×200. The number of capillaries in each field was averaged and expressed as the number of capillary vessels. These morphometric studies were performed by 2 examiners who were blinded to treatment assignment.

Assessment of Cell Differentiation

Suspended MSCs were labeled with fluorescent dyes with use of a PKH26 red fluorescent cell linker kit (Sigma), as reported previously.[17] Fluorescence-labeled MSCs were injected into the myocardium 5 weeks after immunization. Rats (n=5) were humanely killed 4 weeks after cell transplantation. LV samples were embedded in OCT compound, snap-frozen in LN_2, and cut into sections. Immunofluorescence staining was performed with monoclonal mouse anti-cardiac troponin T (Novo), anti-desmin (Dako), anti-connexin-43 (Sigma), polyclonal rabbit anti–von Willebrand factor (Dako), and monoclonal mouse SMA (Dako). FITC-conjugated IgG antibody (BD Pharmingen) was used as a secondary antibody. To perform quantitative analysis of the magnitude of MSC differentiation into cardiomyocytes, heart cells from each rat (n=5) were isolated by incubation in balanced salt solution containing 0.06% collagenase type II (Worthington Biochemical Co), as reported previously.[18] PKH26/troponin T double-positive cells were detected by FACS.

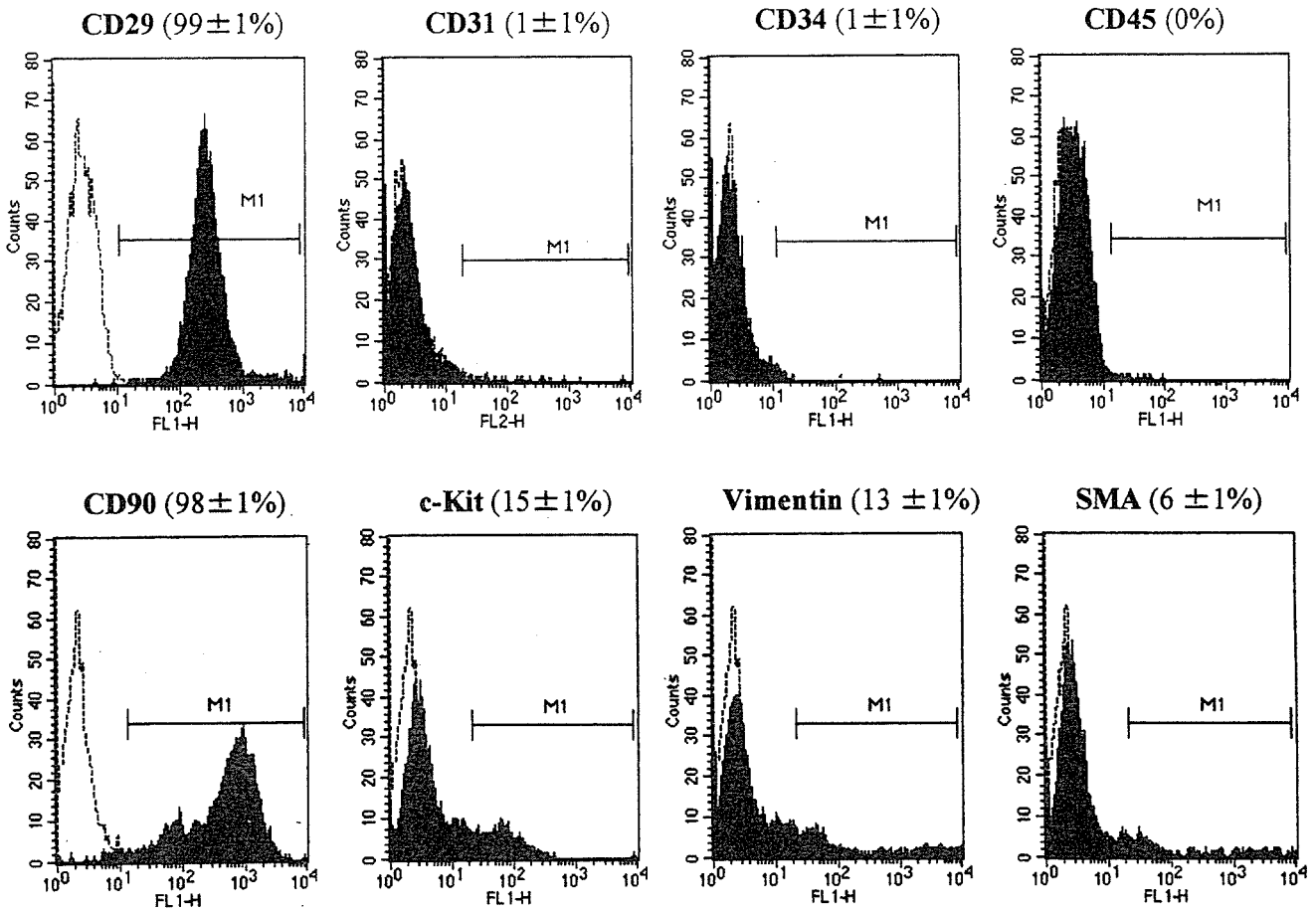

Figure 1. Flow-cytometric analysis of the adherent, spindle-shaped MSC population expanded to 4 to 5 passages. Most of the MSCs expressed CD29 and CD90, whereas they were negative for CD31, CD34, CD45, and SMA. Some of the cells were positive for c-Kit and vimentin.

Western Blot Analysis of Matrix Metalloproteinases

To identify the protein expression of matrix metalloproteinases (MMPs)-2 and -9, Western blotting was performed with rabbit polyclonal antibody raised against MMP-2 (Laboratory vision Co) and MMP-9 (Chemicon Co). The LV obtained from individual rats was used for comparison among the 3 groups (n=5 each). These samples were homogenized on ice in 0.1% Tween 20 homogenization buffer with a protease inhibitor. Then, 40 μg of protein was transferred into sample buffer, loaded on a 7.5% sodium dodecyl sulfate–polyacrylamide gel, and blotted onto a polyvinylidene fluoride membrane (Millipore Co). After being blocked for 120 minutes, the membrane was incubated with primary antibody at a dilution of 1:200. The membrane was incubated with peroxidase labeled with secondary antibody at a dilution of 1:1000. Positive protein bands were visualized with an ECL kit (Amersham) and measured by densitometry. Western blot analysis with a mouse polyclonal antibody raised against β-actin (Santa Cruz) was used as a protein loading control.

Assay for Angiogenic, Antiapoptotic, and Mitogenic Factors

To investigate whether MSCs produce angiogenic and growth factors, we measured VEGF, hepatocyte growth factor (HGF), insulin-like growth factor-1 (IGF-1), and adrenomedullin (AM) levels in conditioned medium 24 hours after medium replacement. VEGF, HGF, and IGF-1 were measured by enzyme immunoassay (VEGF immunoassay, R&D Systems Inc; rat HGF enzyme immunoassay, Institute of Immunology Co, Ltd; and active rat IGF-1 enzyme immunoassay, Diagnostic Systems Laboratories, Inc). AM level was measured with a radioimmunoassay kit (Shionogi Co), as reported previously.[19] The amounts of these products produced by MSCs were compared with those produced by bone marrow–derived mononuclear cells (MNCs) because MNCs have commonly been used for regenerative therapy.[19–21] There was no significant difference in cell viability between MSCs and MNCs 24 hours after seeding (88±5% versus 85±4% by trypan blue solution). In vivo, circulating levels of VEGF, HGF, IGF-1, and AM were measured before and 24 hours after administration of MSCs or vehicle (n=6 from each group).

Statistical Analysis

Numerical values are expressed as mean±SEM unless otherwise indicated. Comparisons of parameters between 2 groups were made with unpaired Student *t* test. Comparisons of parameters among 3 groups were made with a 1-way ANOVA, followed by the Scheffe multiple-comparison test. Comparisons of changes in parameters among the 3 groups were made by a 2-way ANOVA for repeated measures, followed by the Scheffe multiple-comparison test. A value of $P<0.05$ was considered significant.

Results

Characterization of Cultured MSCs

Most cultured MSCs expressed CD29 and CD90 (Figure 1). In contrast, the majority of MSCs were negative for CD31, CD34, CD45, and SMA. Some of the MSCs expressed c-Kit and vimentin.

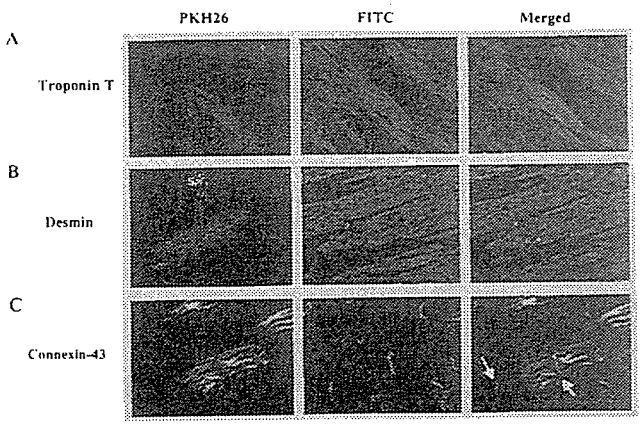

Figure 2. Differentiation of transplanted MSCs into cardiomyocytes. Transplanted MSCs were engrafted in the myocardium and stained for cardiac troponin T (A) and desmin (B). Engrafted MSCs also expressed connexin-43, a gap junction protein, at contact points with native cardiac myocytes (left arrow) and other transplanted cells (right arrow) (C). Magnification ×400.

Myogenesis and Angiogenesis Induced by MSCs

Red fluorescence–labeled MSCs were transplanted into the myocardium 5 weeks after immunization. Four weeks after transplantation, MSCs were engrafted into the myocardium (Figure 2). Immunofluorescence demonstrated that transplanted MSCs were positive for the cardiac markers cardiac troponin T and desmin (Figure 2). Transplanted MSCs also expressed connexin-43, a gap junction protein, at contact points with native cardiac myocytes as well as with MSCs. FACS analysis of isolated heart cells demonstrated that 8±1% of transplanted MSCs were double-positive for PKH26 and troponin T. These results suggest that a small number of transplanted MSCs can differentiate into cardiomyocytes.

Some transplanted MSCs formed vascular structures in the myocardium and were positive for von Willebrand factor (Figure 3A). Other MSCs were positive for SMA and participated in vessel formation as mural cells (Figure 3B). Alkaline phosphatase staining of the ischemic myocardium showed marked augmentation of neovascularization in the MSC-treated DCM group (Figures 4A–4C). Quantitative analysis demonstrated that capillary density was significantly

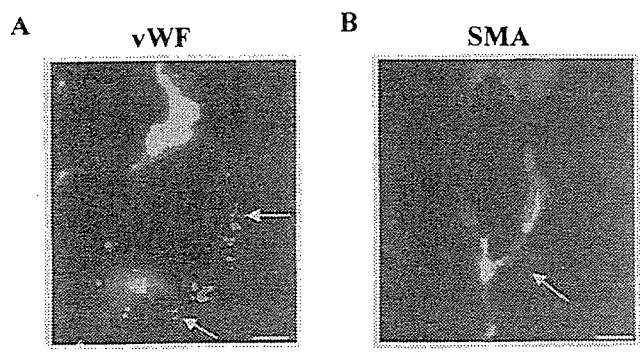

Figure 3. Differentiation of transplanted MSCs into vascular endothelial cells and smooth muscle cells. Some of the transplanted MSCs were positive for von Willebrand factor (vWF, A) and SMA (B) and formed vascular structures (A and B). Scale bars=10 μm.

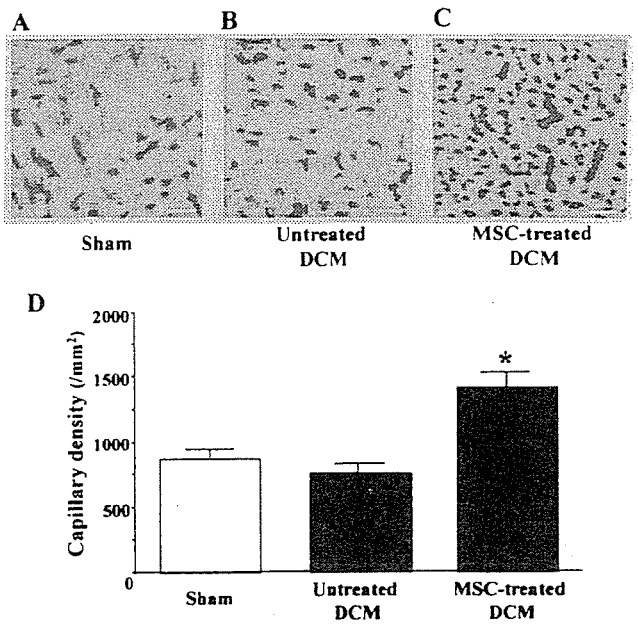

Figure 4. A–C, Representative samples of alkaline phosphatase staining of myocardium. Magnification, ×200. Scale bars=10 μm. D, Quantitative analysis of capillary density in the myocardium. Data are mean±SEM *P<0.05 vs untreated DCM group.

higher in the MSC-treated DCM group than in the untreated DCM group (Figure 4D).

Angiogenic, Antiapoptotic, and Mitogenic Factors Released From MSCs

After 24 hours of culture, MSCs secreted large amounts of angiogenic and antiapoptotic factors, including VEGF, HGF, and AM (Figure 5). Compared with MNCs that have commonly been used for regenerative therapy,[20–22] MSCs secreted 4-fold more VEGF and 5-fold more HGF. Similarly, MSCs secreted 6-fold more AM, an angiogenic and antiapoptotic peptide, compared with MNCs. MSCs also secreted a large amount, 10-fold greater than MNCs, of IGF-1, a growth hormone mediator for myocardial growth (Figure 5). Transplantation of MSCs significantly increased circulating VEGF (45.8±1.6 to 68.5±3.6 pg/mL, P<0.05), HGF (431.8±56.6 to 517.2±67.1 pg/mL, P<0.05), and AM (23.4±0.8 to 41.2±4.8 pg/mL, P<0.05) 24 hours after transplantation, although vehicle injection did not alter these parameters. Serum IGF-1 tended to increase after MSC transplantation (938.1±151.6 to 1063.5±116.9 pg/mL, P=NS), but this increase did not reach statistical significance.

Hemodynamic Effects of MSC Transplantation

Nine weeks after immunization, LV end-diastolic pressure showed a marked elevation in the untreated DCM group; this elevation was significantly attenuated in the MSC-treated DCM group (Figure 6A). LV maximum *dP/dt* was significantly lower in the untreated DCM group than in the sham group (Figure 6B). However, LV maximum *dP/dt* was significantly improved 4 weeks after MSC transplantation. There was no significant difference in heart rate or mean arterial pressure among the 3 groups (the Table). Echocardiographic studies demonstrated LV dysfunction and dilation

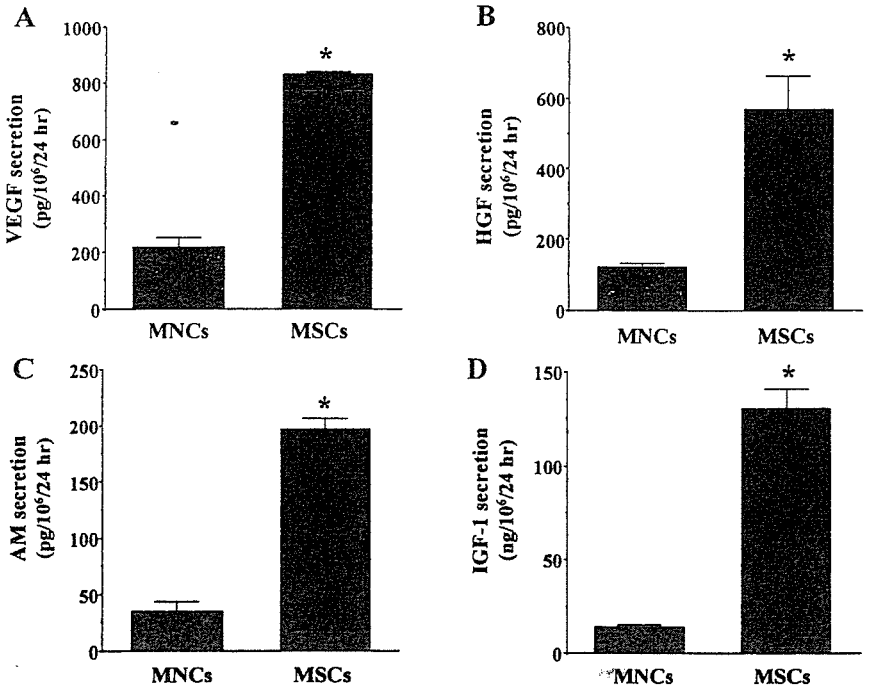

Figure 5. A–D, Angiogenic, antiapoptotic, and mitogenic factors produced by MSCs and bone marrow–derived MNCs). Compared with MNCs, MSCs secreted large amounts of VEGF, HGF, AM, and IGF-1. *$P<0.05$ vs MNCs.

in the untreated DCM group, as indicated by a decrease in percent fractional shortening and an increase in LV diastolic dimension (Figure 6C and 6D). However, MSC transplantation increased percent fractional shortening and inhibited the increase in LV diastolic dimension.

Reduction of Myocardial Fibrosis by MSC Transplantation

Masson's trichrome staining demonstrated modest myocardial fibrosis in the untreated DCM group (Figure 7A). However, MSC transplantation significantly attenuated the development of myocardial fibrosis. Quantitative analysis also demonstrated that the collagen volume fraction in the MSC-treated DCM group was significantly smaller than that in the untreated DCM group (Figure 7B). Western blot analysis showed that myocardial contents of MMP-2 and MMP-9 in the untreated DCM were significantly increased compared with those in the sham group (Figure 7C–E). However, the increases in MMP-2 and MMP-9 levels were attenuated by MSC transplantation, although the change in MMP-9 did not reach statistical significance.

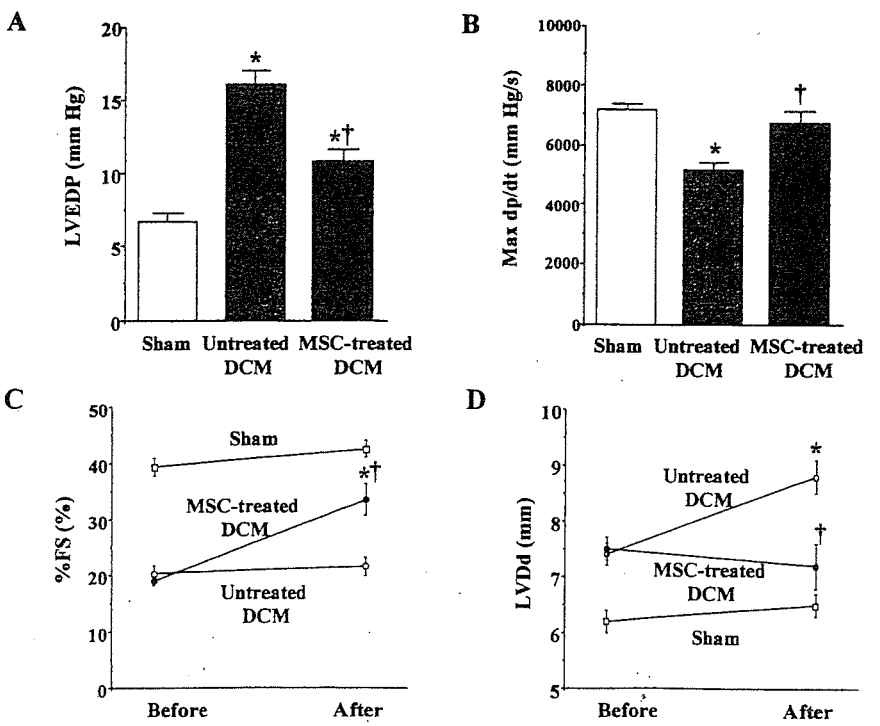

Figure 6. A and B, Effects of MSC transplantation on hemodynamic parameters. LVEDP indicates LV end-diastolic pressure; Max *dP/dt*, LV maximum *dP/dt*. Data are mean±SEM. *$P<0.05$ vs sham group; †$P<0.05$ vs untreated DCM group. C and D, Changes in echocardiographic parameters induced by MSC transplantation. %FS indicates LV fractional shortening. Data are mean±SEM *$P<0.05$ vs before transplantation; †$P<0.05$ vs the time-matched untreated DCM group.

Physiological Profiles of the 3 Experimental Groups

	Sham	Untreated DCM	MSC-Treated DCM
n	10	10	10
Body wt, g	421±8	372±4*	389±5*
LV wt/body wt, g/kg	1.91±0.05	2.18±0.06*	2.05±0.05
RV wt/body wt, g/kg	0.55±0.01	0.68±0.02*	0.60±0.03†
Heart rate, bpm	403±10	432±15	417±12
Mean arterial pressure, mm Hg	134±2	123±3	132±5

wt indicates weight; RV, right ventricle. Sham-operated rats were given vehicle only. The untreated DCM group included DCM rats treated with vehicle. The MSC-treated DCM group included DCM rats treated with MSCs. Data are mean±SEM.

*P<0.05 vs sham group; †P<0.05 vs untreated DCM group.

Discussion

In the present study, we have demonstrated the following effects of MSC transplantation in a rat model of DCM: (1) induction of myogenesis and angiogenesis; (2) differentiation of transplanted MSCs into cardiomyocytes, vascular endothelial cells, and smooth muscle cells; (3) secretion of large amounts of VEGF, HGF, AM, and IGF-1; (4) improvement of cardiac function and inhibition of ventricular remodeling; and (5) decrease in collagen volume fraction in the myocardium.

Earlier studies have shown that transplantation of MSCs improves cardiac function in experimental models of ischemic heart disease.[9,23] However, little information is available about the therapeutic potential of MSCs for chronic heart failure due to DCM. Previous studies have shown that porcine cardiac myosin-induced myocarditis progresses to a chronic phase resembling DCM.[13,14] Thus, we used this model 5 weeks after immunization as an example of experimental DCM.

In the present study, transplanted MSCs were engrafted into the myocardium in a rat model of DCM. Four weeks after transplantation, some of the engrafted MSCs were positively stained for cardiac troponin T and desmin. Transplanted MSCs also expressed connexin-43, a gap junction protein, at contact points with native cardiac myocytes as well as with MSCs. These results suggest that MSCs differentiate into cardiomyocytes in the myocardium and form connections with native cardiomyocytes in rats with DCM. Unlike earlier studies that have used a model of myocardial infarction,[7,9,23] we used a rat model of DCM to demonstrate the engraftment and cardiogenic differentiation of MSCs. Importantly, MSC transplantation improved cardiac function in these rats, as indicated by a significant decrease in LV end-diastolic pressure and an increase in LV dP/dt_{max}. Thus, the improvement in cardiac function may be a result of MSC-induced myocardial regeneration; however, further studies are necessary to investigate the mechanisms by which MSCs develop into cardiac myocyte–like cells.

Some of the transplanted MSCs were positive for a vascular endothelial cell marker and participated in vessel formation. MSC transplantation significantly increased capillary density in the myocardium. SMA staining revealed that MSCs differentiated into vascular smooth muscle cells, which play an important role in vessel maturation. Earlier studies have shown that transplantation of MNCs induces therapeutic angiogenesis in patients with limb ischemia or ischemic heart disease.[20–22] The angiogenic potential of MNCs is mediated at least in part by production by the cells of a variety of angiogenic factors.[24] Although MSCs have also been shown to produce VEGF,[10,25] there has been no study to compare their production between MSCs and MNCs. The present study demonstrated that MSCs secreted ≈4-fold more VEGF compared with MNCs. Furthermore, MSCs secreted large amounts of HGF and AM, potent angiogenic factors.[26–30] Taking these findings together, MSCs may contribute to neovascularization in the myocardium not only through their ability to generate capillary-like structures but also through growth factor–mediated paracrine regulation. Myocardial blood flow abnormalities have been documented in patients with heart failure caused by DCM.[12] Thus, it is possible that MSC-induced neovascularization contributes to improvement in cardiac function.

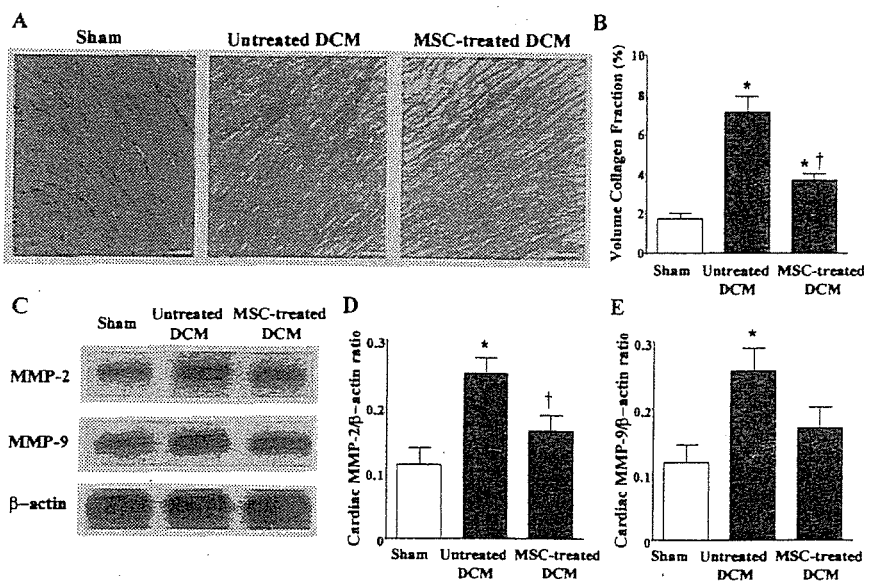

Figure 7. Effects of MSC transplantation on myocardial fibrosis. A, Photomicrographs show representative myocardial sections stained with Masson's trichrome. Scale bars=10 μm. B, Quantitative analysis demonstrated that the collagen volume fraction in the MSC-treated DCM group was significantly smaller than that in the untreated DCM group. C, Representative Western blots for MMPs-2 and -9 and β-actin in the heart. D and E, Quantitative analysis of cardiac tissue contents of MMP-2 and -9. Data are mean±SEM *P<0.05 vs sham group; †P<0.05 vs untreated DCM group.

HGF has not only angiogenic but also cardioprotective effects, including antiapoptotic, mitogenic, and antifibrotic activities.[26,27] *HGF* gene transfer into the myocardium improves myocardial function and geometry.[28] In particular, the antifibrotic effects of HGF through inhibition of transforming growth factor-β expression is beneficial for heart failure. Cultured MSCs secreted a large amount of HGF. In vivo, transplantation of MSCs slightly increased plasma HGF in rats. It significantly attenuated the development of myocardial fibrosis in a rat model of DCM. These results suggest that MSC-derived HGF may contribute to improvements in cardiac function partly through its antifibrotic effects.

MSCs also produced AM, a potent vasodilator and cardioprotective peptide.[29] We have shown that AM prevents cardiomyocyte apoptosis through the phosphatidylinositol 3-kinase/Akt–dependent pathway[16] and that it has potent angiogenic effects.[30] AM inhibits proliferation of cardiac fibroblasts through the cAMP-dependent pathway.[31] Administration of AM inhibits LV remodeling and improves cardiac function in heart failure.[32–34] In the present study, cultured MSCs secreted a large amount of AM in vitro. In vivo, transplantation of MSCs markedly increased plasma AM level. Taken together, these findings suggest that MSCs may exert their cardioprotective effects through AM-mediated paracrine regulation.

IGF-1, a growth hormone mediator, plays an important role in myocardial and skeletal muscle growth.[35,36] Administration of IGF-1 improves cardiac function after myocardial infarction through enhancement of myocardial growth.[37] Its protective and antiapoptotic properties have been demonstrated in different models of myocardial ischemia.[38] Furthermore, IGF-1 exerts Ca^{2+}-dependent, positive inotropic effects through a phosphatidylinositol 3-kinase–dependent pathway.[39] Interestingly, the present study demonstrated that MSCs secreted significant amounts of IGF-1 in vitro, 10-fold greater than MNCs. These findings raise the possibility that MSC-derived IGF-1 may participate in myocardial growth and enhancement of myocardial contractility in a rat model of DCM.

MMPs also play a crucial role in extracellular remodeling in heart failure.[40] In fact, pharmacological inhibition of MMP activities prevents progressive LV remodeling in an animal model of heart failure.[41] In the present study, cardiac MMP-2 and MMP-9 were increased in rats with DCM, which is consistent with recent findings in patients with heart failure.[40,42] Interestingly, MSC transplantation attenuated the increases in cardiac MMP-2 and MMP-9 in a rat model of DCM. Although the underlying mechanisms remain unclear, MSC transplantation may influence extracellular remodeling in heart failure.

The present study has some limitations. First, immunohistochemical evidence suggests differentiation of MSCs into cardiomyocytes, vascular endothelial cells, and smooth muscle cells. However, further studies are necessary to convincingly demonstrate differentiation of MSCs into a specific cell type. Second, the model of DCM used in this study was an injury model, and the effects of treatment may be related to attenuation of the injury rather than to the established cardiomyopathy. Nonetheless, the experiment was performed 5 to 9 weeks after myosin injection, by which time inflammatory changes were hardly observed and had been replaced by fibrosis.[43]

Conclusions

MSC transplantation improved cardiac function in a rat model of DCM, possibly through induction of myogenesis and angiogenesis, as well as by inhibition of myocardial fibrosis. The beneficial effects of MSCs may be mediated at least in part by their differentiation into cardiomyocytes and vascular cells and by their ability to supply large amounts of angiogenic, antiapoptotic, and mitogenic factors. Thus, MSC transplantation has potential as a new therapeutic strategy for the treatment of DCM.

Acknowledgments

This work was supported by research grants for cardiovascular disease (16C-6) and Human Genome Tissue Engineering 009 from the Ministry of Health, Labor and Welfare; the Industrial Technology Research Grant Program in '03 from the New Energy and Industrial Technology Development Organization of Japan; a research grant from the Japan Cardiovascular Research Foundation; and Promotion of Fundamental Studies in Health Science of the Organization for Pharmaceutical Safety and Research of Japan.

References

1. Cohn JN. The management of chronic heart failure. *N Engl J Med.* 1996;335:490–498.
2. Dec GW, Fuster V. Idiopathic dilated cardiomyopathy. *N Engl J Med.* 1994;331:1564–1575.
3. Beltrami AP, Urbanek K, Kajstura J, Yan SM, Finato N, Bussani R, Nadal-Ginard B, Silvestri F, Leri A, Beltrami CA, Anversa P. Evidence that human cardiac myocytes divide after myocardial infarction. *N Engl J Med.* 2001;344:1750–1757.
4. Pittenger MF, Mackay AM, Beck SC, Jaiswal RK, Douglas R, Mosca JD, Moorman MA, Simonetti DW, Craig S, Marshak DR. Multilineage potential of adult human mesenchymal stem cells. *Science.* 1999;284:143–147.
5. Reyes M, Dudek A, Jahagirdar B, Koodie L, Marker PH, Verfaillie CM. Origin of endothelial progenitors in human postnatal bone marrow. *J Clin Invest.* 2002;109:337–346.
6. Toma C, Pittenger MF, Cahill KS, Byrne BJ, Kessler PD. Human mesenchymal stem cells differentiate to a cardiomyocyte phenotype in the adult murine heart. *Circulation.* 2002;105:93–98.
7. Mangi AA, Noiseux N, Kong D, He H, Rezvani M, Ingwall JS, Dzau VJ. Mesenchymal stem cells modified with Akt prevent remodeling and restore performance of infarcted hearts. *Nat Med.* 2003;9:1195–1201.
8. Makino S, Fukuda K, Miyoshi S, Konishi F, Kodama H, Pan J, Sano M, Takahashi T, Hori S, Abe H, Hata J, Umezawa A, Ogawa S. Cardiomyocytes can be generated from marrow stromal cells in vitro. *J Clin Invest.* 1999;103:697–705.
9. Shake JG, Gruber PJ, Baumgartner WA, Senechal G, Meyers J, Redmond JM, Pittenger MF, Martin BJ. Mesenchymal stem cell implantation in a swine myocardial infarct model: engraftment and functional effects. *Ann Thorac Surg.* 2002;73:1919–1925.
10. Al-Khaldi A, Al-Sabti H, Galipeau J, Lachapelle K. Therapeutic angiogenesis using autologous bone marrow stromal cells: improved blood flow in a chronic limb ischemia model. *Ann Thorac Surg.* 2003;75:204–209.
11. Al-Khaldi A, Eliopoulos N, Martineau D, Lejeune L, Lachapelle K, Galipeau J. Postnatal bone marrow stromal cells elicit a potent VEGF-dependent neoangiogenic response in vivo. *Gene Ther.* 2003;10:621–629.
12. Parodi O, De Maria R, Oltrona L, Testa R, Sambuceti G, Roghi A, Merli M, Belingheri L, Accinni R, Spinelli F, Pellegrini A, Baroldi G. Myocardial blood flow distribution in patients with ischemic heart disease or dilated cardiomyopathy undergoing heart transplantation. *Circulation.* 1993;88:509–522.
13. Kodama M, Zhang S, Hanawa H, Saeki M, Inomata T, Suzuki K, Koyama S, Shibata A. Effects of 15-deoxyspergualin on experimental autoimmune giant cell myocarditis of the rat. *Circulation.* 1995;91:1116–1122.
14. Watanabe K, Ohta Y, Nakazawa M, Higuchi H, Hasegawa G, Naito M, Fuse K, Ito M, Hirono S, Tanabe N, Hanawa H, Kato K, Kodama M, Aizawa Y. Low dose carvedilol inhibits progression of heart failure in rats with dilated cardiomyopathy. *Br J Pharmacol.* 2000;130:1489–1495.

15. Nagaya N, Uematsu M, Kojima M, Ikeda Y, Yoshihara F, Shimizu W, Hosoda H, Hirota Y, Ishida H, Mori H, Kangawa K. Chronic administration of ghrelin improves left ventricular dysfunction and attenuates development of cardiac cachexia in rats with heart failure. *Circulation*. 2001;104:1430–1435.
16. Okumura H, Nagaya N, Itoh T, Okano I, Hino J, Mori K, Tsukamoto Y, Ishibashi-Ueda H, Miwa S, Tambara K, Toyokuni S, Yutani C, Kangawa K. Adrenomedullin infusion attenuates myocardial ischemia/reperfusion injury through the phosphatidylinositol 3-kinase/Akt-dependent pathway. *Circulation*. 2004;109:242–248.
17. Messina LM, Podrazik RM, Whitehill TA, Ekhterae D, Brothers TE, Wilson JM, Burkel WE, Stanley JC. Adhesion and incorporation of lacZ-transduced endothelial cells into the intact capillary wall in the rat. *Proc Natl Acad Sci U S A*. 1992;89:12018–12022.
18. Harada M, Itoh H, Nakagawa O, Ogawa Y, Miyamoto Y, Kuwahara K, Ogawa E, Igaki T, Yamashita J, Masuda I, Yoshimasa T, Tanaka I, Saito Y, Nakao K. Significance of ventricular myocytes and nonmyocytes interaction during cardiocyte hypertrophy: evidence for endothelin-1 as a paracrine hypertrophic factor from cardiac nonmyocytes. *Circulation*. 1997;96:3737–3744.
19. Ohta H, Tsuji T, Asai S, Sasakura K, Teraoka H, Kitamura K, Kangawa K. A simple immunoradiometric assay for measuring the entire molecules of adrenomedullin in human plasma. *Clin Chim Acta*. 1999;287:B131–B143.
20. Murohara T, Ikeda H, Duan J, Shintani S, Sasaki K, Eguchi H, Onitsuka I, Matsui K, Imaizumi T. Transplanted cord blood-derived endothelial precursor cells augment postnatal neovascularization. *J Clin Invest*. 2000; 105:1527–1536.
21. Tateishi-Yuyama E, Matsubara H, Murohara T, Ikeda U, Shintani S, Masaki H, Amano K, Kishimoto Y, Yoshimoto K, Akashi H, Shimada K, Iwasaka T, Imaizumi T. Therapeutic Angiogenesis using Cell Transplantation (TACT) Study Investigators. Therapeutic angiogenesis for patients with limb ischaemia by autologous transplantation of bone-marrow cells: a pilot study and a randomised controlled trial. *Lancet*. 2002;360:427–435.
22. Tse HF, Kwong YL, Chan JK, Lo G, Ho CL, Lau CP. Angiogenesis in ischaemic myocardium by intramyocardial autologous bone marrow mononuclear cell implantation. *Lancet*. 2003;4:47–49.
23. Min JY, Sullivan MF, Yang Y, Zhang JP, Converso KL, Morgan JP, Xiao YF. Significant improvement of heart function by cotransplantation of human mesenchymal stem cells and fetal cardiomyocytes in postinfarcted pigs. *Ann Thorac Surg*. 2002;74:1568–1575.
24. Kamihata H, Matsubara H, Nishiue T, Fujiyama S, Tsutsumi Y, Ozono R, Masaki H, Mori Y, Iba O, Tateishi E, Kosaki A, Shintani S, Murohara T, Imaizumi T, Iwasaka T. Implantation of bone marrow mononuclear cells into ischemic myocardium enhances collateral perfusion and regional function via side supply of angioblasts, angiogenic ligands, and cytokines. *Circulation*. 2001;104:1046–1052.
25. Kinnaird T, Stabile E, Burnett MS, Lee CW, Barr S, Fuchs S, Epstein SE. Marrow-derived stromal cells express genes encoding a broad spectrum of arteriogenic cytokines and promote in vitro and in vivo arteriogenesis through paracrine mechanisms. *Circ Res*. 2004;94:678–685.
26. Nakamura T, Nishizawa T, Hagiya M, Seki T, Shimonishi M, Sugimura A, Tashiro K, Shimizu S. Molecular cloning and expression of human hepatocyte growth factor. *Nature*. 1989;342:440–443.
27. Nakamura T, Mizuno S, Matsumoto K, Sawa Y, Matsuda H, Nakamura T. Myocardial protection from ischemia/reperfusion injury by endogenous and exogenous HGF. *J Clin Invest*. 2000;106:1511–1519.
28. Li Y, Takemura G, Kosai K, Yuge K, Nagano S, Esaki M, Goto K, Takahashi T, Hayakawa K, Koda M, Kawase Y, Maruyama R, Okada H, Minatoguchi S, Mizuguchi H, Fujiwara T, Fujiwara H. Postinfarction treatment with an adenoviral vector expressing hepatocyte growth factor relieves chronic left ventricular remodeling and dysfunction in mice. *Circulation*. 2003;107:2499–2506.
29. Kitamura K, Kangawa K, Kawamoto M, Ichiki Y, Nakamura S, Matsuo H, Eto T. Adrenomedullin: a novel hypotensive peptide isolated from human pheochromocytoma. *Biochem Biophys Res Commun*. 1993;192:553–560.
30. Tokunaga N, Nagaya N, Shirai M, Tanaka E, Ishibashi-Ueda H, Harada-Shiba M, Kanda M, Ito T, Shimizu W, Tabata Y, Uematsu M, Nishigami K, Sano S, Kangawa K, Mori H. Adrenomedullin gene transfer induces therapeutic angiogenesis in a rabbit model of chronic hind limb ischemia: benefits of a novel nonviral vector, gelatin. *Circulation*. 2004;109:526–531.
31. Tsuruda T, Kato J, Kitamura K, Kawamoto M, Kuwasako K, Imamura T, Koiwaya Y, Tsuji T, Kangawa K, Eto T. An autocrine or a paracrine role of adrenomedullin in modulating cardiac fibroblast growth. *Cardiovasc Res*. 1999;43:958–967.
32. Nishikimi T, Yoshihara F, Horinaka S, Kobayashi N, Mori Y, Tadokoro K, Akimoto K, Minamino N, Kangawa K, Matsuoka H. Chronic administration of adrenomedullin attenuates transition from left ventricular hypertrophy to heart failure in rats. *Hypertension*. 2003;42:1034–1041.
33. Nakamura R, Kato J, Kitamura K, Onitsuka H, Imamura T, Cao Y, Marutsuka K, Asada Y, Kangawa K, Eto T. Adrenomedullin administration immediately after myocardial infarction ameliorates progression of heart failure in rats. *Circulation*. 2004;110:426–431.
34. Nagaya N, Satoh T, Nishikimi T, Uematsu M, Furuichi S, Sakamaki F, Oya H, Kyotani S, Nakanishi N, Goto Y, Masuda Y, Miyatake K, Kangawa K. Hemodynamic, renal, and hormonal effects of adrenomedullin infusion in patients with congestive heart failure. *Circulation*. 2000;101:498–503.
35. Fuller J, Mynett JR, Sugden PH. Stimulation of cardiac protein synthesis by insulin-like growth factors. *Biochem J*. 1992;282:85–90.
36. Florini JR, Ewton DZ, Coolican SA. Growth hormone and the insulin-like growth factor system in myogenesis. *Endocr Rev*. 1996;17:481–517.
37. Cittadini A, Stromer H, Katz SE, Clark R, Moses AC, Morgan JP, Douglas PS. Differential cardiac effects of growth hormone and insulin-like growth factor-1 in the rat: a combined in vivo and in vitro evaluation. *Circulation*. 1996;93:800–809.
38. Li Q, Li B, Wang X, Leri A, Jana KP, Liu Y, Kajstura J, Baserga R, Anversa P. Overexpression of insulin-like growth factor-1 in mice protects from myocyte death after infarction, attenuating ventricular dilation, wall stress, and cardiac hypertrophy. *J Clin Invest*. 1997;100:1991–1999.
39. von Lewinski D, Voss K, Hulsmann S, Kogler H, Pieske B. Insulin-like growth factor-1 exerts Ca^{2+}-dependent positive inotropic effects in failing human myocardium. *Circ Res*. 2003;92:169–176.
40. Thomas CV, Coker ML, Zellner JL, Handy JR, Crumbley AJ 3rd, Spinale FG. Increased matrix metalloproteinase activity and selective upregulation in LV myocardium from patients with end-stage dilated cardiomyopathy. *Circulation*. 1998;97:1708–1715.
41. Spinale FG, Coker ML, Krombach SR, Mukherjee R, Hallak H, Houck WV, Clair MJ, Kribbs SB, Johnson LL, Peterson JT, Zile MR. Matrix metalloproteinase inhibition during the development of congestive heart failure: effects on left ventricular dimensions and function. *Circ Res*. 1999;85:364–376.
42. Spinale FG, Coker ML, Heung LJ, Bond BR, Gunasinghe HR, Etoh T, Goldberg AT, Zellner JL, Crumbley AJ. A matrix metalloproteinase induction/activation system exists in the human left ventricular myocardium and is upregulated in heart failure. *Circulation*. 2000;102:1944–1949.
43. Kodama M, Matsumoto Y, Fujiwara M, Zhang SS, Hanawa H, Itoh E, Tsuda T, Izumi T, Shibata A. Characteristics of giant cells and factors related to the formation of giant cells in myocarditis. *Circ Res*. 1991;69:1042–1050.

CLINICAL PERSPECTIVE

Transplantation of stem or progenitor cells has the potential to improve and restore cardiac function. To date, experimenters investigating the possible therapeutic effects of stem cells in the heart have used models of infarction, and little information is available about the therapeutic potential of cell transplantation for heart failure due to dilated cardiomyopathy. In the present study, we demonstrated that transplantation of stem cells improved cardiac function in a model of myocarditis. We found evidence that stem cells may work to improve heart function by both myogenesis and angiogenesis while inhibiting myocardial fibrosis. Based on our data, part of the mechanism for this improvement may occur through the action of stem cells as a source of growth factors and cytokines in the heart. This study supports the overall notion that mesenchymal stem cells transplanted into the failing heart have potential as a new therapeutic strategy for the treatment of dilated cardiomyopathy.

THE JOURNAL OF BIOLOGICAL CHEMISTRY VOL. 281, NO. 11, pp. 7205–7213, March 17, 2006

Functions of the Cytoplasmic Tails of the Human Receptor Activity-modifying Protein Components of Calcitonin Gene-related Peptide and Adrenomedullin Receptors*[S]

Received for publication, October 13, 2005, and in revised form, January 6, 2006 Published, JBC Papers in Press, January 11, 2006, DOI 10.1074/jbc.M511147200

Kenji Kuwasako[‡1], Yuan-Ning Cao[‡], Chun-Ping Chu[§], Shuji Iwatsubo[‡], Tanenao Eto[‡], and Kazuo Kitamura[‡]

From the [‡]First and [§]Third Departments of Internal Medicine, Miyazaki Medical College, University of Miyazaki, Miyazaki 889-1692, Japan

Receptor activity-modifying proteins (RAMPs) enable calcitonin receptor-like receptor (CRLR) to function as a calcitonin gene-related peptide receptor (CRLR/RAMP1) or an adrenomedullin (AM) receptor (CRLR/RAMP2 or -3). Here we investigated the functions of the cytoplasmic C-terminal tails (C-tails) of human RAMP1, -2, and -3 (hRAMP1, -2, and -3) by cotransfecting their C-terminal deletion or progressive truncation mutants into HEK-293 cells stably expressing hCRLR. Deletion of the C-tail from hRAMP1 had little effect on the surface expression, function, or intracellular trafficking of the mutant heterodimers. By contrast, deletion of the C-tail from hRAMP2 disrupted transport of hCRLR to the cell surface, resulting in significant reductions in ^{125}I-hAM binding and evoked cAMP accumulation. The transfection efficiency for the hRAMP2 mutant was comparable with that for wild-type hRAMP2; moreover, immunocytochemical analysis showed that the mutant hRAMP2 remained within the endoplasmic reticulum. FACS analysis revealed that deleting the C-tail from hRAMP3 markedly enhances AM-evoked internalization of the mutant heterodimers, although there was no change in agonist affinity. Truncating the C-tails by removing the six C-terminal amino acids of hRAMP2 and -3 or exchanging their C-tails with one another had no effect on surface expression, agonist affinity, or internalization of hCRLR, which suggests that the highly conserved Ser-Lys sequence within hRAMP C-tails is involved in cellular trafficking of the two AM receptors. Notably, deleting the respective C-tails from hRAMPs had no effect on lysosomal sorting of hCRLR. Thus, the respective C-tails of hRAMP2 and -3 differentially affect hCRLR surface delivery and internalization.

CGRP[2] and AM belong to the calcitonin family of regulatory molecules and exert a wide variety of biological effects, including potent vasorelaxation (1–3). The receptors that mediate these effects are heterodimers composed of CRLR and RAMP, a novel accessory protein (4). The three RAMP isoforms (RAMP1, RAMP2, and RAMP3) are each composed of ~160 amino acids, and all exhibit a common structure that includes a large extracellular N-terminal domain, a single membrane-spanning domain, and a very short C-tail, but they share less than 30% sequence identity and differ in their tissue distributions (4, 5). When acting as a chaperone, each RAMP forms a 1:1 heterodimer with CRLR, probably in the ER (4, 6). They then mediate the transport of CRLR to the cell surface, where the heterodimers form functional CGRP or AM receptors: CRLR/RAMP1 forms the $CGRP_1$ receptor (4), which can also be activated by high concentrations of AM (7, 8); CRLR/RAMP2 forms an AM-specific receptor that is sensitive to the AM receptor antagonist AM-(22–52) (AM_1 receptor) (7, 9); and CRLR/RAMP3 forms an AM receptor that is sensitive to both the $CGRP_1$ receptor antagonist CGRP-(8–37) and AM-(22–52) (AM_2 receptor) (7, 9). It is the RAMP extracellular domain that mediates agonist binding to CRLR/RAMP heterodimers (11–13), which in turn mediate intracellular cAMP production and Ca^{2+} mobilization (4, 10).

Exposing cells that express GPCRs to their respective agonists frequently leads to a rapid internalization of the receptor in a process believed to involve clathrin-coated vesicles, caveolin-rich vesicles, or both (14, 15). The internalized GPCRs may be recycled back to the plasma membrane in order to promote functional restoration of signal transduction, or they may be trafficked to lysosomes, where they are degraded (14, 15). Similarly, upon binding their respective agonist, hCRLR/RAMP heterodimers stably expressed in HEK-293 cells are rapidly internalized without dissociation via clathrin-coated vesicles (6, 10) in a process that is blocked by dominant negative mutants of dynamin and β-arrestin 2 (6). In that regard, it is well known that G protein-coupled receptor kinases phosphorylate serine/threonine sites located in many GPCR C-tails, enabling β-arrestins to bind there (16). After internalization, both CRLR and RAMP are targeted to lysosomes (10), where they are degraded (6).

Although short, the RAMP C-tails do contain potential sites of interaction with other proteins (5, 17). For instance, the hRAMP3 C-tail possesses a classical type I PDZ (PSD-95/Disc-large/ZO-1) binding motif (TLL) (5, 17), and the binding of NSF to the PDZ motif of hRAMP3 was found to promote slow recycling of internalized hCRLR/hRAMP3 heterodimers in HEK-293 cells (18). In addition, a five-residue motif (QSKRT) in the hRAMP1 C-tail can act as an ER retention signal (19). The C-tails of RAMPs, like that of CRLR, also contain potential phosphorylation and ubiquitination sites (5, 17). Ubiquitination is the post-translational attachment of ubiquitin lysine residues in the substrate proteins (20, 21); it is not crucial for receptor internalization but is essential for proper trafficking to lysosomes for degradation (22, 23). Whether the phosphorylation and ubiquitination sites are also involved

* This work was supported in part by grants-in-aid for scientific research on priority areas and for the 21st Century Centers of Excellence Program (Life Science) from the Ministry of Education, Culture, Sports, Science, and Technology, Japan. The costs of publication of this article were defrayed in part by the payment of page charges. This article must therefore be hereby marked "*advertisement*" in accordance with 18 U.S.C. Section 1734 solely to indicate this fact.

[S] The on-line version of this article (available at http://www.jbc.org) contains one supplemental figure.

[1] To whom correspondence should be addressed. Tel.: 81-985-85-0872; Fax: 81-985-85-6596; E-mail: kuwasako@fc.miyazaki-med.ac.jp.

[2] The abbreviations used are: CGRP, calcitonin gene-related peptide; hαCGRP, human αCGRP; AM, adrenomedullin; hAM, human AM; CRLR, calcitonin receptor-like receptor; hCRLR, human CRLR; RAMP, receptor activity-modifying protein; C-tail, cytoplasmic C-terminal tail; ER, endoplasmic reticulum; GPCRs, G protein-coupled receptors; NSF, *N*-ethylmaleimide-sensitive factor; hNSF, human NSF; PDZ, PSD-95/Disc-large/ZO-1; FITC, fluorescein isothionate; PE, phycoerythrin; HEK, human embryonic kidney; GFP, green fluorescent protein; FACS, fluorescence-activated cell sorting; PBS, phosphate-buffered saline; NHERF, Na^+/H^+ exchanger regulatory factor; β_2-AR, β_2-adrenergic receptor.

in intracellular trafficking of CRLR/RAMP heterodimers remains unknown. To address that issue, we examined the effects of expressing various hRAMP C-tail deletion and progressive truncation mutants and chimeras in which the C-tails were exchanged among the three hRAMPs in HEK-293 cells stably expressing hCRLR.

EXPERIMENTAL PROCEDURES

Materials—^{125}I-[Tyr^0]hαCGRP (specific activity 2 μCi/pmol) (24), which contains an extra N-terminal tyrosine residue (Tyr^0), and ^{125}I-hAM (specific activity 2 μCi/pmol) (1) were both produced in our laboratory. Human αCGRP was purchased from Peptide Institute (Osaka, Japan). [Tyr^0]hαCGRP was from Phoenix Pharmaceuticals, Inc. Human AM was kindly donated by Shionogi & Co. (Osaka, Japan). Mouse anti-hNSF antibody was from Calbiochem. Mouse anti-V5 antibody and FITC-conjugated mouse anti-V5 monoclonal antibody (anti-V5-FITC antibody) were from Invitrogen. Rabbit anti-calnexin antibody was from Stressgen Biotechnologies Corp. (Victoria, Canada), and Alexa Fluor® 594 (biotin- and fluorescent dye-labeled goat anti-rabbit IgG antibody) were from Molecular Probes, Inc. (Eugene, OR). PE-conjugated rabbit anti-mouse secondary antibody was from Exalpha Biologicals, Inc. All other reagents were of analytical grade and were obtained from various commercial suppliers.

Expression Constructs—hNSF (GenBank™ accession number BC030613) was cloned from cDNA obtained from human heart (Clontech) using PCR with the appropriate primers and then modified to provide a consensus Kozak sequence as previously described (25). hRAMP1, -2, and -3 (4) were also modified to provide the same Kozak sequence. A double V5 epitope tag (GKPIPNPLLGLDST) was ligated, in frame, to the 5′-end of the cDNAs encoding each intact hRAMP, and the native signal sequences were removed and replaced with MKTILALSTYIFCLVFA (26), yielding V5-hRAMP1, -2, and -3. The deletion and progressive truncation mutations in the V5-hRAMP C-tails were created by using 3′-primers that introduced a translational stop codon at the desired positions (Fig. 1); with RAMP3, for instance, Δ139 represents a mutant in which a stop codon was introduced after residue 139. In addition, various V5-hRAMP chimeras were constructed by exchanging the 9 C-terminal amino acid residues among the three hRAMPs. The hNSF, V5-hRAMPs, V5-hRAMP deletion and truncation mutants, and V5-hRAMP chimeras were then respectively cloned into the mammalian expression vector pCAGGS/Neo (10) using the 5′-XhoI and 3′-NotI sites, and the sequences of the resultant constructs were all verified using an Applied Biosystems 310 Genetic Analyzer. The individual V5-hRAMPs were compared with the native sequence in the assays and were found to behave identically (data not shown).

Cell Culture and DNA Transfection—HEK-293 cells stably expressing a hCRLR-GFP chimera (10) were maintained in Dulbecco's modified Eagle's medium supplemented with 10% fetal bovine serum, 100 units/ml penicillin G, 100 μg/ml streptomycin, 0.25 μg/ml amphotericin B, and 0.25 mg/ml G 418 at 37 °C under a humidified atmosphere of 95% air, 5% CO_2. For experimentation, cells were seeded into 6- or 24-well plates and, upon reaching 70 – 80% confluence, were transiently cotransfected with the indicated cDNAs using Lipofectamine transfection reagents (Invitrogen) according to the manufacturer's instructions. Briefly, the cells were incubated for 4 h in Opti-MEM I medium containing plasmid DNAs, Plus reagent, and Lipofectamine (see Ref. 27 for 6-well and Ref. 11 for 24-well plates). As a control, some cells were transfected with empty vector (mock). All experiments were carried out 48 h after transfection.

FACS Analysis—Flow cytometry was carried out to assess the levels of cell surface expression of V5-hRAMPs, V5-hRAMP truncation mutants, or V5-hRAMP chimeras in HEK-293 cells. To evaluate cell surface expression, cells were harvested following transient transfection, washed twice with PBS, resuspended in ice-cold FACS buffer (27), and then incubated for 60 min at 4 °C in the dark with anti-V5 monoclonal antibody (1:1000 dilution). Following two additional washes with FACS buffer, the cells were incubated for 60 min at 4 °C in the dark with PE-conjugated rabbit anti-mouse secondary antibody (1:400 dilution) in ice-cold FACS buffer. For evaluation of whole cell expression, cells were first permeabilized using IntraPrep™ reagents (Beckman Coulter, Fullerton, CA) according to the manufacturer's instructions and then incubated with anti-V5-FITC antibody (1:500 dilution) for 15 min at room temperature in the dark. Following two successive washes with FACS buffer, both groups of cells were subjected to flow cytometry in an EPICS XL flow cytometer (Beckman Coulter) and analyzed using EXPO 2 software (Beckman Coulter). Fluorophores were excited at 488 nm, and the emission was monitored at 530 nm for GFP and 575 nm for PE. Viability was assessed by exclusion of propidium iodide.

Immunofluorescence Microscopy—HEK-293 cells stably expressing hCRLR-GFP were plated onto 35-mm glass-bottomed dishes (Iwaki, Tokyo, Japan). As determined by the experimental protocol, some cells were then transiently transfected with V5-hRAMP2, Δ166-hRAMP2, or Δ167-hRAMP2. The cells were then fixed with 3.7% formaldehyde in PBS for 20 min at room temperature, washed twice with PBS, and permeabilized with 0.25% Triton X-100 in PBS for 10 min. Thereafter, the cells were incubated at room temperature for 30 min in blocking buffer (PBS containing 1% bovine serum albumin), followed by incubation for 60 min first with rabbit anti-calnexin (1:200 dilution) and mouse anti-V5-FITC antibody (1:500 dilution) and then, after washing four times with PBS, with the Alexa Fluor® 594 diluted 1:100 in blocking buffer. After another three washes with PBS, the cells were mounted using Slow-Fade mounting medium (Molecular Probes, Inc.), and a 22-mm glass coverslip was seated in the center of each dish. Double labeling was

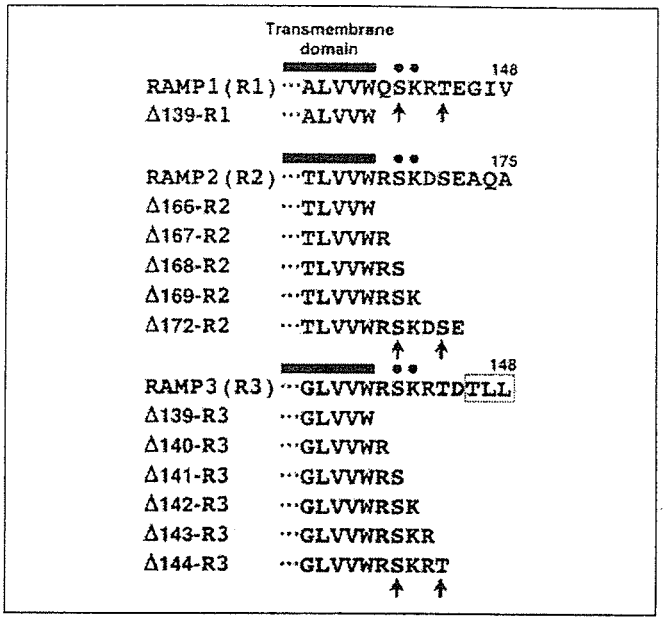

FIGURE 1. **Amino acid sequence alignment of the cytoplasmic tails of hRAMP1, -2, and -3.** The sequences are aligned for maximum homology; alignment of the entire sequences was presented by MacLatchie *et al.* (4). The *numbers* indicate the amino acid positions in accordance with Sexton *et al.* (5). *Black circles* indicate conserved amino acids; *arrows* indicate potential phosphorylation sites; and the PDZ binding motif is *boxed*. The progressive hRAMP C-tail truncation mutants were created using 3′-primers that introduced a translational stop codon at the indicated positions; for instance, Δ139 represents a truncation mutant that introduced a stop codon after residue 139.

viewed using a TCS-SP2 AOBS confocal laser-scanning microscope (Leica) equipped with a × 63/1.32 numerical aperture immersion lens (Leica).

Whole-cell Radioligand Binding Assays—Transfected HEK-293 cells in 24-well plates were washed twice with prewarmed PBS and then incubated for 5 h at 4 °C with ^{125}I-[Tyr^0]hαCGRP (100 pM) or ^{125}I-hAM (20 pM) in the presence (for nonspecific binding) or absence (for total binding) of 1 μM unlabeled hαCGRP or hAM in modified Krebs-Ringer-HEPES medium (10), after which they were washed twice more with ice-cold PBS and harvested with 0.5 M NaOH. The associated cellular radioactivity was measured in a γ-counter. Specific binding was defined as the difference between total binding and nonspecific binding.

cAMP Measurements—Transfectants in 24-well plates were incubated for 15 min at 37 °C in Hanks' buffer containing 20 mM HEPES, 0.2% bovine serum albumin, 0.5 mM 3-isobutyl-1-methylxanthine (Sigma), and the indicated concentrations of hαCGRP or hAM. The reaction mixture was then replaced with 20 mM HCl and 1 M acetic acid to extract the intracellular cAMP, after which the resultant extracts were lyophilized and stored at −30 °C until assayed. The cAMP concentrations were measured using our specific radioimmunoassay (1).

FACS Analysis of Receptor Internalization and Recycling—Following cotransfection of the indicated cDNAs into HEK-293 cells stably expressing hCRLR-GFP in 6-well plates, the cells were exposed to selected concentrations of hαCGRP or hAM in prewarmed serum-free Dulbecco's modified Eagle's medium containing 20 mM HEPES and 0.2% bovine serum albumin for the indicated periods (up to 2 h) at 37 °C. For receptor recycling studies, the cells were incubating for 60 min with the agonist plus 10 μg/ml cycloheximide and 10 μg/ml brefeldin A and then washed three times with prewarmed PBS. The medium was then replaced with prewarmed Dulbecco's modified Eagle's medium containing 20 mM HEPES, 10% fetal bovine serum, 10 μg/ml cycloheximide, and 10 μg/ml brefeldin A for the indicated periods (up to 4 h) at 37 °C. Internalization and recycling were stopped by adding ice-cold PBS, after which the cells were harvested, resuspended in ice-cold FACS buffer, and labeled with anti-V5 monoclonal antibody and fluorescein PE-conjugated rabbit anti-mouse secondary antibody. The cells were then subjected to flow cytometry and analyzed as described above.

mRNA Expression Measured by Real Time Quantitative PCR—Total RNAs were extracted from HEK-293 cells either untransfected or transfected as indicated using total RNA isolation reagent (Invitrogen). Thereafter, the target cDNAs were synthesized from the respective mRNAs by reverse transcription using SuperScript reverse transcriptase (Invitrogen). The expression of mRNAs encoding hNSF was assessed using real time quantitative PCR (Prism 7700 Sequence Detector, Applied Biosystems, Foster City, CA) with original oligonucleotide primers (sense, 5′-AGAACAGTGACCGCACACCAT-3′; antisense, 5′-TCCACAACCACACAACTGAGC-3′) and a fluorescently labeled probe (5′-AGCGTGCTTCTGGAAGGCCCTCCTCACAGT-3′). The size of the amplified DNA was 223 bp. The levels of hNSF mRNA were normalized to those of glyceraldehyde-3-phosphate dehydrogenase mRNA, which served as an internal control.

Western Analysis—Following transient transfection of hNSF into cells plated in 6-well plates, the transfectants were washed twice with ice-cold PBS, harvested in 1 ml of sample buffer (28), and boiled for 10 min. Equal aliquots of protein (20 μg) were then subjected to 10% SDS gel electrophoresis and transferred to a Hybond-P membrane (Amersham Biosciences). The membrane was then blocked with 5% block reagent (Amersham Biosciences), washed, and incubated first for 1 h at room temperature with rabbit anti-hNSF antibody (1:1,000 dilution) and then with secondary antibody (1:10,000 dilution). hNSF proteins were detected using an ECL Plus chemiluminescence kit (Amersham Biosciences), after which they were quantitated by densitometry using Image Gauge (LAS-1000; Fujifilm).

Statistical Analysis—Results are expressed as means ± S.E. of at least three independent experiments. Differences between two groups were evaluated using Student's *t* tests; differences among multiple groups were evaluated with a one-way analysis of variance followed by Scheffe's tests. Values of $p < 0.05$ were considered significant.

RESULTS

Deletion of hRAMP C-tails—We previously established HEK-293 cells stably expressing hCRLR-GFP alone or together with Myc-hRAMPs and used them to visualize the cellular localization and trafficking of hCRLR (10). Following AM exposure, hCRLR is rapidly internalized together with its associated hRAMP, and then both are trafficked to lysosomes; fusion of GFP to the C terminus of hCRLR had no apparent effect on the trafficking of the heterodimeric receptor. In the present study, therefore, we used HEK-293 cells stably expressing hCRLR-GFP to examine the functions of the C-tails of the three hRAMPs within the respective CRLR/RAMP heterodimers.

We initially tested the effect of completely deleting the C-tails of the three V5-epitope tagged hRAMPs (Fig. 2). When coexpressed with hCRLR, V5-RAMP1, -2, and -3 were detected at the surfaces of 45.9, 21.9, and 38.9% of cells, respectively. On the other hand, the V5-RAMP deletion mutants Δ139-RAMP1, Δ166-RAMP2, and Δ139-RAMP3 appeared at the surface of 43.7, 5.0, and 38.8% of cells, respectively. Thus, deletion of the C-tail significantly reduced surface delivery of only RAMP2. Surface immunoreactivity was detected in only 0.55% of cells expressing the empty vector (Mock), which is well within the 2% limit of resolution characteristic of FACS analysis.

We next evaluated the binding profiles of ^{125}I-[Tyr^0]hαCGRP and ^{125}I-hAM to cells expressing each of the wild-type and mutant receptors (Fig. 3, *A* and *B*). When CRLR-GFP was coexpressed with empty vector (*Mock*), the cells showed only very low levels of specific binding of ^{125}I-[Tyr^0]αCGRP and ^{125}I-AM. Co-transfection of RAMP1 led to markedly higher specific ^{125}I-[Tyr^0]αCGRP binding than was seen with Δ139-RAMP1 (Fig. 3*A*), although there was no difference in the surface expression of either heterodimeric receptor (Fig. 2). Likewise, cotransfection of RAMP2 significantly increased the specific binding of

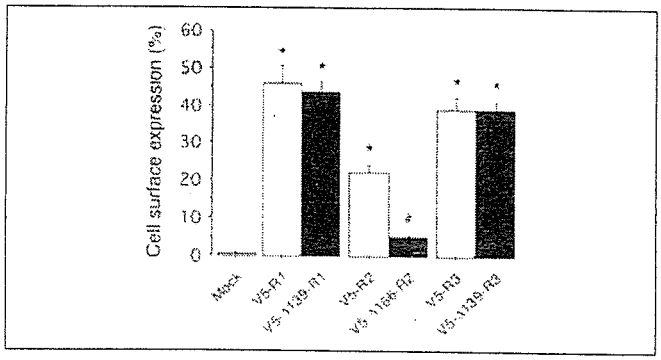

FIGURE 2. **FACS analysis of HEK-293 cells coexpressing hCRLR with intact hRAMP or a C-terminal deletion mutant.** HEK-293 cells stably expressing CRLR-GFP were transiently transfected with empty vector (*Mock*) or the indicated V5-RAMP or deletion mutant. The cells were incubated first with an anti-V5 monoclonal antibody and then with a fluorescein PE-conjugated rabbit anti-mouse secondary antibody. Samples incubated with only secondary antibody served as the control. Cell surface expression of each construct was estimated by flow cytometry. The *bars* represent means ± S.E. of six independent experiments. *, $p < 0.001$ *versus* control (*Mock*); #, $p < 0.02$ *versus* corresponding wild-type V5-RAMP.

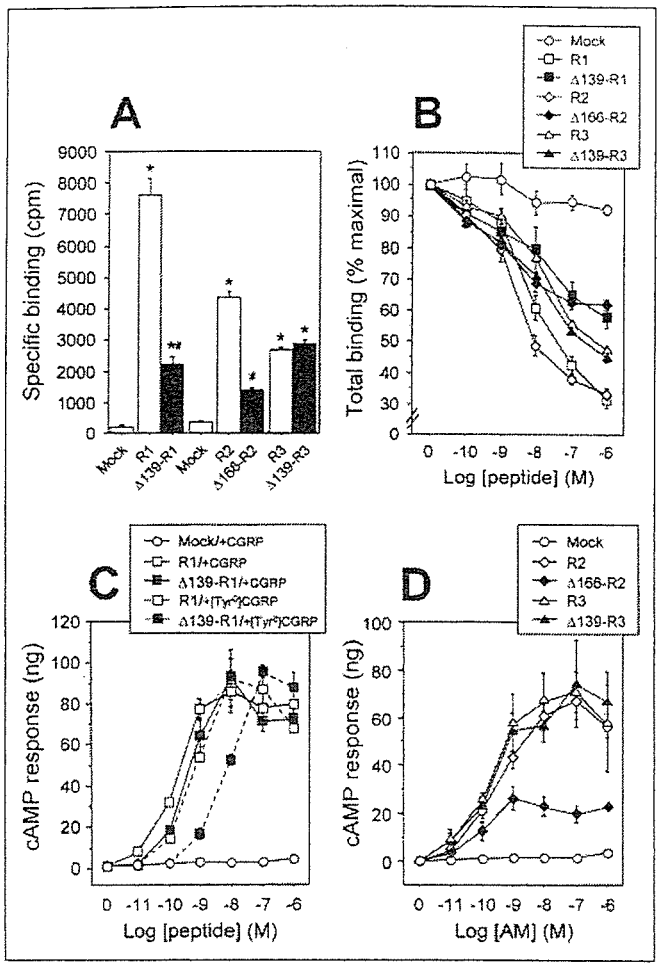

FIGURE 3. **Effects of hRAMP C-terminal deletion on agonist binding and evoked cAMP production in HEK-293 cells stably expressing hCRLR.** *A*, specific binding of ^{125}I-hαCGRP and ^{125}I-hAM. HEK-293 cells expressing CRLR-GFP were transiently transfected with empty vector (*Mock*) or the indicated V5-RAMP or deletion mutant, after which the cells were incubated for 5 h at 4 °C with ^{125}I-αCGRP (100 pM) or ^{125}I-AM (20 pM) in the presence or absence of 1 μM unlabeled αCGRP or AM. *Bars* represent means ± S.E. of three experiments. *, $p < 0.002$ *versus* Mock; #, $p < 0.001$ *versus* corresponding wild-type V5-RAMP. *B*, displacement of radioligand. Cells were transfected and radiolabeled as in *A* either alone or with the indicated concentration of unlabeled ligand (αCGRP or AM). *Bars* represent means ± S.E. of three experiments. *C* and *D*, evoked cAMP production. After transient transfection of V5-RAMPs and the corresponding deletion mutants, cells were exposed to the indicated concentrations of αCGRP, [Tyr^0]αCGRP, or AM for 15 min at 37 °C and then lysed. The resultant lysates were analyzed for cAMP content. *Bars* represent means ± S.E. of three experiments.

^{125}I-AM to CRLR-GFP-expressing cells, whereas cotransfection of Δ166-RAMP2 did not. In this case, the reduced binding could be due to reduced surface delivery of the mutant receptors (Fig. 2). Finally, deletion of the RAMP3 C-tail had no effect on specific ^{125}I-AM binding.

Fig. 3*B* shows a set of ^{125}I-[Tyr^0]αCGRP and ^{125}I-AM competition curves for the wild-type and mutant receptors. The IC_{50} values derived from the curves obtained with cotransfection of Δ139-RAMP1 or Δ166-RAMP2 were both >1000 nM, which is much higher than those for RAMP1 and -2 (43.0 and 12.2 nM, respectively). By contrast, the IC_{50} values obtained with expression of RAMP3 or Δ139-RAMP3 were within the same order of magnitude (560 and 257 nM, respectively).

We then further characterized the mutant receptors by measuring agonist-induced intracellular cAMP accumulation (Fig. 3, *C* and *D*). αCGRP and AM elicited little or no cAMP production in HEK-293 cells expressing CRLR-GFP alone, indicating that the stable transfectants used in this study express no functional RAMP proteins. In cells coexpressing RAMP1 and CRLR-GFP, by contrast, αCGRP (EC_{50} = 0.18 nM) elicited marked increases in cAMP (Fig. 3*C*). In cells expressing Δ139-RAMP1 with CRLR-GFP, the EC_{50} for αCGRP was increased only a little, as compared with RAMP1 (to 0.49 nM), and the maximal responses were also similar to those seen with RAMP1 (Fig. 3*C*). Interestingly, the responses to [Tyr^0]αCGRP by cells expressing CRLR-GFP/Δ139-RAMP1 (EC_{50} = 8.5 nM) were significantly smaller than those seen in cells expressing CRLR-GFP/RAMP1 (EC_{50} = 0.79 nM). In cells transfected with RAMP2, AM elicited significant increases in cAMP (EC_{50} = 0.38 nM), but these responses were diminished by 62.1% in cells transfected with Δ166-RAMP2, although there was no significant change in EC_{50} (0.16 nM) (Fig. 3*D*). AM-evoked cAMP production did not significantly differ in cells expressing RAMP3 or Δ139-RAMP3 (EC_{50} = 0.41 and 0.20 nM, respectively) (Fig. 3*D*). That the cAMP production elicited via the respective receptors largely paralleled the profile of radioligand binding (Fig. 3, *A* and *B*) suggests that the C-tails of RAMP1 and -3 have little or no involvement with agonist binding and signaling.

We previously quantified the internalization and recycling of AM receptors (CRLR/RAMP heterodimers) using radioligand binding assays; however, interpretation of those experiments was complicated by the high degree of nonspecific AM binding, which reflected the highly hydrophobic and basic nature of the native peptide (1, 10, 11). In the present study, therefore, we used FACS to evaluate agonist-mediated internalization and recycling of wild-type and mutant CRLR-GFP/RAMP heterodimers. Fig. 4*A* shows the receptor internalization induced by 1 μM αCGRP- or AM. Exposure to the appropriate agonist elicited rapid declines in cell surface expression of wild-type CRLR-GFP/RAMP1 and -3 that led to 40–60% reductions in signal strength within 2 h and to 90% reduction in cell surface CRLR-GFP/RAMP2 within 30 min. Heterodimers composed of CRLR-GFP plus Δ139-RAMP1 or Δ166-RAMP2 tended to be internalized somewhat less efficiently, whereas internalization of the CRLR-GFP/Δ139-RAMP3 heterodimer was markedly enhanced. Notably, these phenomena occurred with no changes in cell surface CRLR-GFP expression or AM binding and signaling (Figs. 2 and 3).

The dose dependence of the agonist-evoked receptor internalization is illustrated in Fig. 4*B*. αCGRP elicited equivalent dose-dependent internalization of CRLR-GFP/RAMP1 and CRLR-GFP/Δ139-RAMP1. AM dose-dependently induced RAMP2-mediated internalization of CRLR-GFP, which was more efficient than RAMP1-mediated internalization. And Δ166-RAMP2 mediated internalization of CRLR-GFP even more efficiently than did wild-type RAMP2, although the basal surface expression of CRLR-GFP/Δ166-RAMP2 was much lower (Fig. 2*A*). Δ139-RAMP3-mediated internalization of CRLR-GFP only differed from that mediated by wild-type RAMP3 at high AM concentrations (100 nM and 1 μM), at which time internalization of the mutant was more efficient.

Progressive Truncation of the C-Tails of hRAMP2 and -3—The results presented so far show that for hRAMP1, the C-tail is not necessary for cell surface delivery and internalization of CRLR (Figs. 2 and 4). For hRAMP2 and -3, by contrast, the respective C-tails do appear to be involved in determining the surface expression and internalization kinetics of CRLR.

To determine more precisely which sites on the C-tails of hRAMP2 and -3 regulate the cellular trafficking of CRLR/RAMP heterodimers, we constructed a group of progressive C-tail truncation mutants (Fig. 1) and then transfected each RAMP construct into HEK-293 cells stably expressing CRLR-GFP. When Δ166- or Δ167-RAMP2 was individually transfected into HEK-293 cells, its transfection efficiency (~15%) was

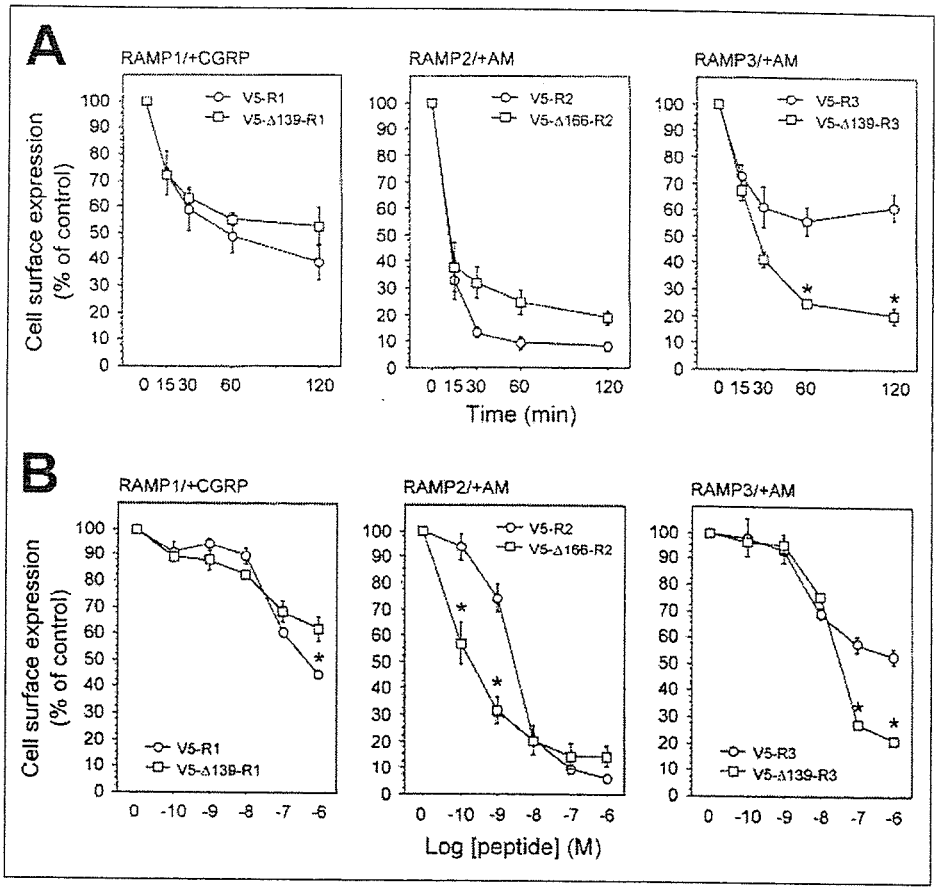

FIGURE 4. **FACS analysis of the time course of agonist-induced internalization of hCRLR with hRAMPs or their C-terminal deletion mutants.** *A*, time-dependent loss of surface CRLR/RAMP heterodimers. HEK-293 cells stably expressing CRLR-GFP were transiently transfected with V5-RAMPs or their C-terminal deletion mutants and then treated with 1 μM αCGRP or AM for the indicated times. Cell surface expression of each construct was estimated by flow cytometry. The *symbols* represent means ± S.E. of three independent experiments; *, $p < 0.006$ *versus* control. *B*, agonist-evoked internalization of hCRLR with hRAMPs or their deletion mutants. Each transfectant was incubated for 60 min with the indicated concentrations of αCGRP or AM. Cell surface expression of each construct was estimated by flow cytometry. *Symbols* represent means ± S.E. of three independent experiments; *, $p < 0.03$ *versus* control.

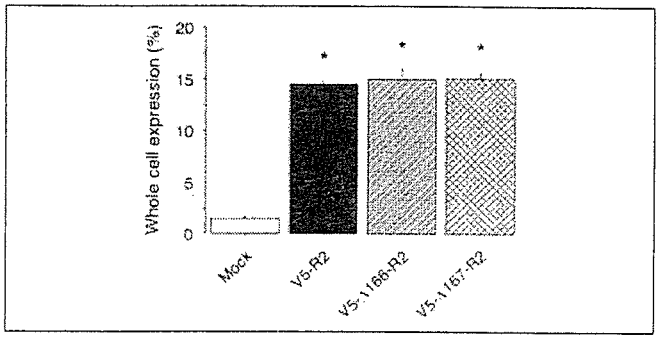

FIGURE 5. **FACS analysis of whole cell expression of hRAMP2 and its truncation mutants.** The indicated RAMP constructs were transiently transfected into HEK-293 cells. Forty-eight hours after transfection, cells were permeabilized with IntraPrep™ reagent and then incubated for 15 min at room temperature with anti-V5-FITC antibody; mock incubation with the antibody served as the control. Whole cell expression of each construct was estimated by flow cytometry. The *symbols* represent means ± S.E. of three independent experiments; *, $p < 0.001$ *versus* control.

comparable with that for wild-type RAMP2 (Fig. 5). Moreover, immunocytochemical analysis showed that almost all of both mutants remained in the ER, representing a pool of newly synthesized molecules not yet transported to the cell surface (Fig. 6). Although they were transfected into CRLR-GFP-expressing cells, however, Δ166- and Δ167-RAMP2 largely failed to transport CRLR-GFP to the cell surface, resulting in significant reductions in specific ^{125}I-AM binding and AM-evoked cAMP production (Table 1). This suggests that the 168th and 169th amino acids (SK sequence) of RAMP2 are important for cell surface delivery of CRLR. The reason for the discrepancy between the IC_{50} and EC_{50} remains unclear, however. By contrast, Δ168- and Δ169-RAMP mediated substantially greater levels of cell surface CRLR-GFP expression, so that AM binding and signaling were equivalent to that seen with wild-type RAMP2 (Table 1). All of the RAMP3 truncation mutants appeared together with CRLR-GFP at the cell surface (Fig. 6*A*), and the resultant receptors showed AM binding and signaling that was comparable with that seen with wild-type RAMP3 (Table 1).

Among the RAMP2 mutants, Δ166 significantly reduced internalization of CRLR-GFP (Fig. 7). Conversely, the Δ139- and Δ140-RAMP3 mutants mediated significantly greater CRLR-GFP internalization than wild-type RAMP3 (Fig. 7). Such increases were not seen with Δ141-RAMP3, and CRLR-GFP internalization mediated by Δ142, Δ143, and Δ144 was equal to that seen with wild-type RAMP3. Thus, the presence of amino acids 141 and 142 (SK sequence) of RAMP3 leads to significant decreases in CRLR internalization.

Characteristics of hRAMP C-tail Chimeras—The SK sequence is highly conserved in the C-tails of all three hRAMPs (Fig. 1) as well as in RAMP isoforms from other species (17). We therefore tested whether exchanging C-tails would affect the cellular trafficking of CRLR-GFP. Given that hRAMP2 promoted CRLR internalization more effectively than other hRAMP isoforms did and that there were no differences in CRLR surface delivery and internalization by hRAMP1 and -3, we constructed four RAMP chimeras (RAMP1/2, -2/1, -2/3, and -3/2) by taking advantage of unique restriction sites that enabled us to generate four hybrid genes. These RAMP chimeras were then transiently transfected into HEK293 cells stably expressing CRLR-GFP and characterized by FACS analysis. As shown in Table 2, cell surface expression and evoked CRLR-GFP internalization of all four chimeras was comparable with

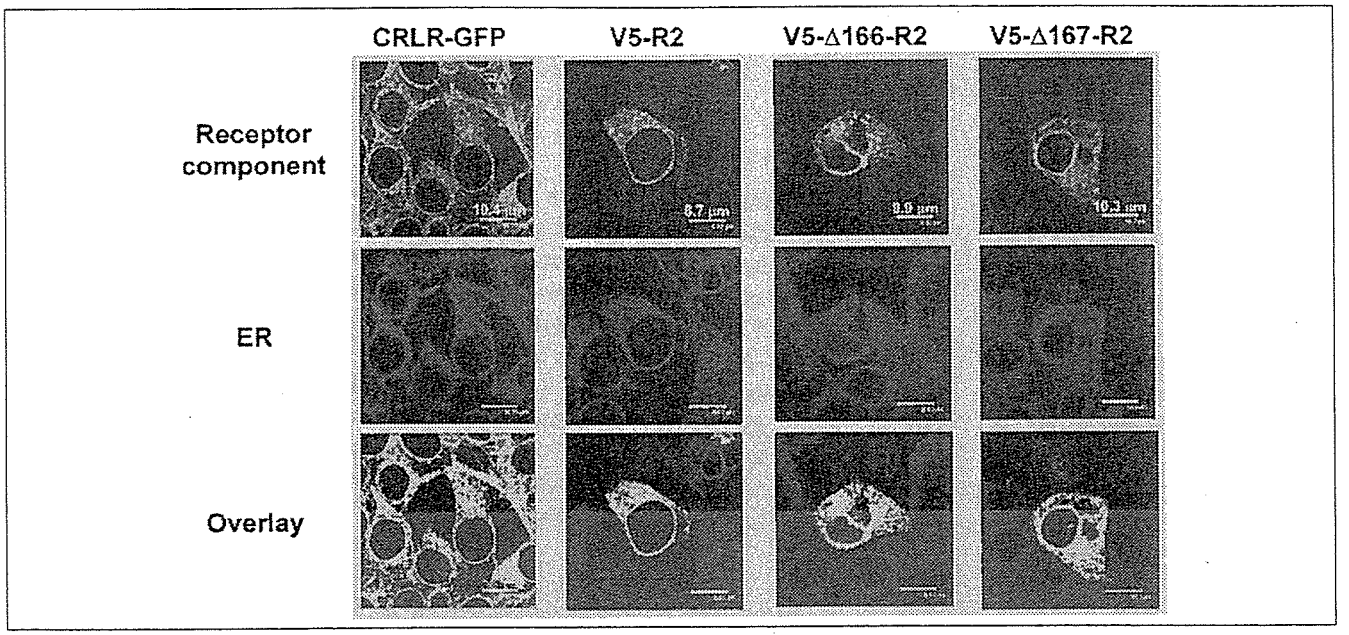

FIGURE 6. **Intracellular localization of V5-hRAMP2 and its truncation mutants.** The indicated RAMP2 constructs were transiently transfected into HEK-293 cells, after which their subcellular distribution was assessed by confocal microscopy in permeabilized cells using anti-V5-FITC antibody. Calnexin (for the ER) was visualized using the appropriate secondary antibody (Alexa Fluor® 594). Co-localization with the ER marker was determined by overlay of the images (*lower panels*). HEK-293 cells stably expressing CRLR-GFP served as the control for co-localization of CRLR-GFP and the ER (*left panels*). *Bar*, ~10 μm.

TABLE 1

Characterization of HEK-293 cells expressing CRLR-GFP and progressive V5-RAMP2 and -3 truncation mutants

The indicated RAMP constructs were transiently transfected into CRLR-GFP-expressing HEK-293 cells. Surface expression of each construct was estimated by flow cytometry. The results represent the means ± S.E. of three independent experiments.

	Cell surface expression (% V5-RAMP2 or -3)	^{125}I-AM binding		AM-evoked cAMP production	
		IC_{50}	Specific binding (% V5-RAMP2 or -3)	EC_{50}	Maximal responses (% V5-RAMP2 or -3)
	%	nM	%	nM	%
V5-RAMP2 (R2)	100	12.2 ± 5.0	100	0.38 ± 0.14	100
V5-Δ166-R2	14.6 ± 1.5[a]	>1000	31.8 ± 1.4[a]	0.16 ± 0.07	37.9 ± 4.7[a]
V5-Δ167-R2	29.0 ± 2.3[a]	>1000	48.0 ± 2.9[a]	0.21 ± 0.09	52.3 ± 1.8[a]
V5-Δ168-R2	61.7 ± 5.5	13.7 ± 5.3	98.4 ± 7.2	0.26 ± 0.22	73.8 ± 20.5
V5-Δ169-R2	83.6 ± 7.8	12.9 ± 3.5	95.8 ± 3.9	0.10 ± 0.06	87.8 ± 19.3
V5-Δ172-R2	55.9 ± 8.1	18.0 ± 6.0	83.1 ± 2.4[a]	0.24 ± 0.04	61.5 ± 4.9
V5-RAMP3 (R3)	100	560 ± 100	100	0.41 ± 0.25	100
V5-Δ139-R3	89.3 ± 6.0	257 ± 49	107 ± 4.3	0.20 ± 0.08	93.8 ± 12.1
V5-Δ140-R3	79.7 ± 5.3	687 ± 70	93.9 ± 1.7	2.50 ± 1.49	91.0 ± 5.7
V5-Δ141-R3	89.1 ± 11.6	317 ± 73	114 ± 1.3[a]	0.30 ± 0.14	116 ± 7.5
V5-Δ142-R3	79.4 ± 9.7	483 ± 193	114 ± 4.5	0.98 ± 0.31	101 ± 8.6
V5-Δ143-R3	84.0 ± 12.8	386 ± 307	111 ± 11.4	0.38 ± 0.21	113 ± 21.6
V5-Δ144-R3	78.2 ± 10.3	383 ± 105	114 ± 6.1	0.13 ± 0.09	102 ± 12.1

[a] $p < 0.03$ *versus* corresponding control (V5-RAMP2 or -3).

that seen with the respective wild-type RAMPs. Thus, exchanging C-tails did not affect RAMP-mediated surface delivery or internalization of CRLR.

Effect of hRAMP C-tail Deletion on Receptor Recycling—For recycling studies, cells were pretreated with 10 μg/ml cycloheximide and 10 μg/ml brefeldin A to respectively inhibit *de novo* protein synthesis and cause disassembly of the Golgi apparatus (29); neither of these reagents had any effect of their own on CGRP- or AM-induced internalization of CRLR-GFP/RAMPs (data not shown). Subsequent treatment of cells with 1 μM αCGRP or AM for 60 min elicited a loss of cell surface receptors that persisted for at least 2 h after washing out the ligands (Fig. 8*A*). Very similar results were seen with Δ139-RAMP1, Δ166-RAMP2, and Δ139-RAMP3, suggesting the RAMP C-tails are not involved in lysosomal sorting of CRLR or the binding of protein(s) that determine the fate of internalized receptors.

Internalization and Recycling of AM_2 Receptors in Cells Cotransfected with hNSF—It was recently shown that, unlike NHERF, NSF contains no recognizable PDZ domains (30) but nonetheless interacts with the PDZ motif of hRAMP3, enabling internalized AM_2 receptors to undergo slow recycling (18). Conversely, NSF enhances β-arrestin 1-mediated β_2-AR internalization (31). Notably, although rat and mouse RAMP3 C-tails contain a RLL sequence instead of a PDZ motif, NSF also promotes recycling of these CRLR/RAMP3 heterodimers (18). With the aim of better understanding the role of NSF in AM_2 receptor trafficking, in the present study, we tested whether the reported effects of hNSF on CRLR/RAMP3 trafficking are reproduced in HEK-293 cells endogenously expressing hNSF and in hNSF transfectants.

We first confirmed that NSF was indeed endogenously expressed in HEK-293 cells by identifying both NSF mRNA and protein in the

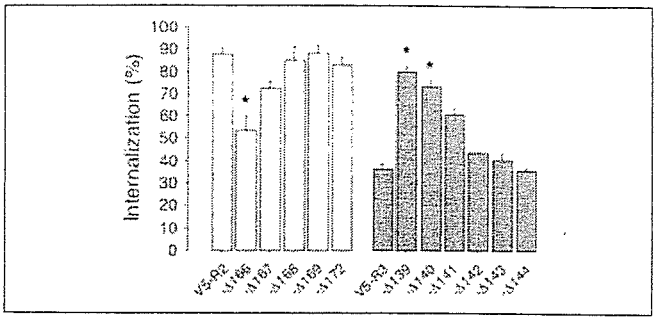

FIGURE 7. **FACS analysis of internalization of hCRLR with progressive hRAMP2 and -3 truncation mutants.** The indicated RAMP constructs were transiently transfected into CRLR-GFP-expressing HEK-293 cells. Surface expression of each construct was estimated by flow cytometry before and after exposing cells to 1 μM AM for 60 min. The results represent the means ± S.E. of three independent experiments; *, $p < 0.003$ *versus* corresponding control (V5-RAMP2 or -3).

TABLE 2

FACS analysis of cell surface delivery and internalization of CRLR-GFP and V5-RAMP chimeras in which the C-tails were exchanged among the three RAMPs

The indicated V5-RAMPs or their chimeras were transiently transfected into CRLR-GFP-expressing HEK-293 cells. Surface expression of each construct was estimated by flow cytometry before and after exposing cells to 1 μM αCGRP or AM for 60 min. The results represent the means ± S.E. of three independent experiments.

	Cell surface expression	Internalization
	%	%
V5-RAMP1	51.8 ± 3.7	50.0 ± 4.3
V5-RAMP2	23.2 ± 2.7	94.5 ± 1.6
V5-RAMP3	46.3 ± 4.8	35.5 ± 1.8
V5-RAMP1/2	49.7 ± 5.6	53.7 ± 7.2
V5-RAMP2/1	25.8 ± 2.3	91.8 ± 0.4
V5-RAMP2/3	19.5 ± 1.4	88.2 ± 1.2
V5-RAMP3/2	44.9 ± 6.1	36.7 ± 3.8

cells (Fig. 8, *B* and *C*). Thereafter, we determined that the levels of the transcript were unaffected by transfection of CRLR-GFP alone or together with V5-RAMP3 (Fig. 8*D*). When NSF was transfected into otherwise untransfected HEK-293 cells and into CRLR-GFP transfectants, levels of its transcript were markedly higher than their endogenous levels in both (Fig. 8*B*). In those cases, Western analysis of NSF protein yielded a single, strong 76-kDa band that was identical to the band obtained when endogenous NSF was probed (Fig. 8*C*), which confirmed that our NSF transfection system worked appropriately. Exposure to 10 nM or 1 μM AM for 60 min induced a rapid decline in cell surface CRLR-GFP/V5-RAMP3 that persisted for at least 4 h after washing out the AM (Fig. 8*D*). Cotransfection of NSF had no effect on these internalization kinetics, and recycling of CRLR/RAMP3 heterodimers, if it occurred, was highly inefficient, even in the presence of abundant NSF (Fig. 8*D*).

DISCUSSION

Since their discovery, there have been only a few reports addressing the functions of the respective C-tails of the three RAMP isoforms (17–19, 32, 33); more extensively studied have been their extracellular domains (11–13, 17, 32, 34, 35). Consequently, whereas nearly all highly conserved residues are known to play key roles in the function and trafficking of cell surface receptors, nothing is known about the functions of the highly conserved Ser and Lys resides within RAMP C-tails. In the present study, we showed that deleting the C-tail from RAMP3 (Δ139-RAMP3) significantly enhanced AM-induced CRLR-GFP internalization but did not affect the targeting of CRLR-GFP to the cell surface or AM binding and signaling. It is therefore unlikely that the truncation of RAMP3 promoted AM-induced conformational changes in the heterodimeric receptors that would alter the binding of AM and/or the interaction of the receptor with G proteins. On the other hand, like wild-type RAMP3, all of the tested RAMP3 truncation mutants that contained the SK sequence (Δ142-, Δ143-, and Δ144-RAMP3) mediated CRLR-GFP internalization less efficiently than those that did not (Δ139-, Δ140-, or Δ141-RAMP3). We also found that substituting the RAMP3 C-tail with the RAMP2 C-tail, which also contains a SK sequence, had no effect on the AM-induced CRLR-GFP internalization. Taken together, these results suggest that the SK sequence participates in the negative regulation of CRLR/RAMP3 internalization.

The Ser/Thr residues present in the C-tails of the three RAMP have been thought to be potential phosphorylation sites, but Hilairet *et al.* (6) showed that in HEK-293 cells overexpressing CRLR/RAMP heterodimers, agonists rapidly promote phosphorylation of CRLR but not RAMP. They also demonstrated that internalization of the heterodimeric receptors was dependent on β-arrestins (6). In the present study, complete removal of the respective RAMP C-tails did not diminish the maximal extent of internalization. It therefore seems unlikely that β-arrestins interact with the RAMP C-tails.

Similar in function to the SK sequence, a dileucine (LL) motif, which is conserved among GPCRs (36), is also present in the C-tail of RAMP3. This motif negatively regulates lutropin/choriogonadotropin receptor (LHR) internalization, since leucine-to-alanine mutations increased the agonist-stimulated internalization of the receptor (37). It is thought that the LL motif participates in protein sorting through direct interaction with two clathrin adaptor protein (AP) complexes, AP-1 and AP-2 (38–40), and the point mutations disrupted the interaction of the LHR with AP-2 at the plasma membrane (39). On the other hand, these mutations are believed to enhance the binding of β-arrestins to the LHR, thereby promoting bridge formation between β-arrestins and clathrin (37). We suggest that, instead of β-arrestins, the RAMP3 C-tail may interact with other intracellular proteins similar to LRP6, another GPCR accessory protein that interacts with axin and catinin (41).

We believe it is noteworthy that the hRAMP3 C-tail contains not only a LL sequence but also a type I PDZ binding sequence (see Fig. 1). Recently, NHERF-1 was found to interact with the PDZ motif of hRAMP3, resulting in complete inhibition of CRLR/RAMP3 internalization (33). In that case, NHERF-1 is thought to act by tethering surface AM_2 receptors to the actin cytoskeleton in a manner also seen with epidermal growth factor receptors (42). By contrast, NHERF-1 promotes the agonist-mediated recycling of β_2-ARs, which also have a PDZ motif (SLL) (30). The mechanism by which NHERF-1 exerts these differing effects on different GPCRs remains unknown. In the present study, three RAMP3 truncation mutants (Δ142-, Δ143-, and Δ144-RAMP3) and the RAMP3/2 chimera, all of which lack both the LL and PDZ sequences, failed to enhance the AM-induced CRLR-GFP internalization. However, this does not preclude the possibility that the level of endogenous NHERF-1 expression in HEK-293 cells used was insufficient to modulate the behavior of the overexpressed RAMP3.

We also showed that deleting the C-tail of RAMP2 impaired the targeting of the CRLR-GFP to the cell surface, thereby markedly reducing AM binding and signaling. Most of the newly synthesized Δ166-RAMP2 remained in the ER along with CRLR-GFP. By contrast, removing the C-tail from RAMP1 or -3 did not diminish surface delivery of the respective receptors. All of the RAMP2 mutants containing an SK sequence (Δ168-, Δ169-, and Δ172-RAMP2) showed better surface CRLR-GFP expression than was seen with Δ166-RAMP2, which lacked the SK sequence. Apparently, the SK sequence in the RAMP2 C-tail is involved in the proper membrane localization of the CRLR/RAMP2. To our knowledge, there have

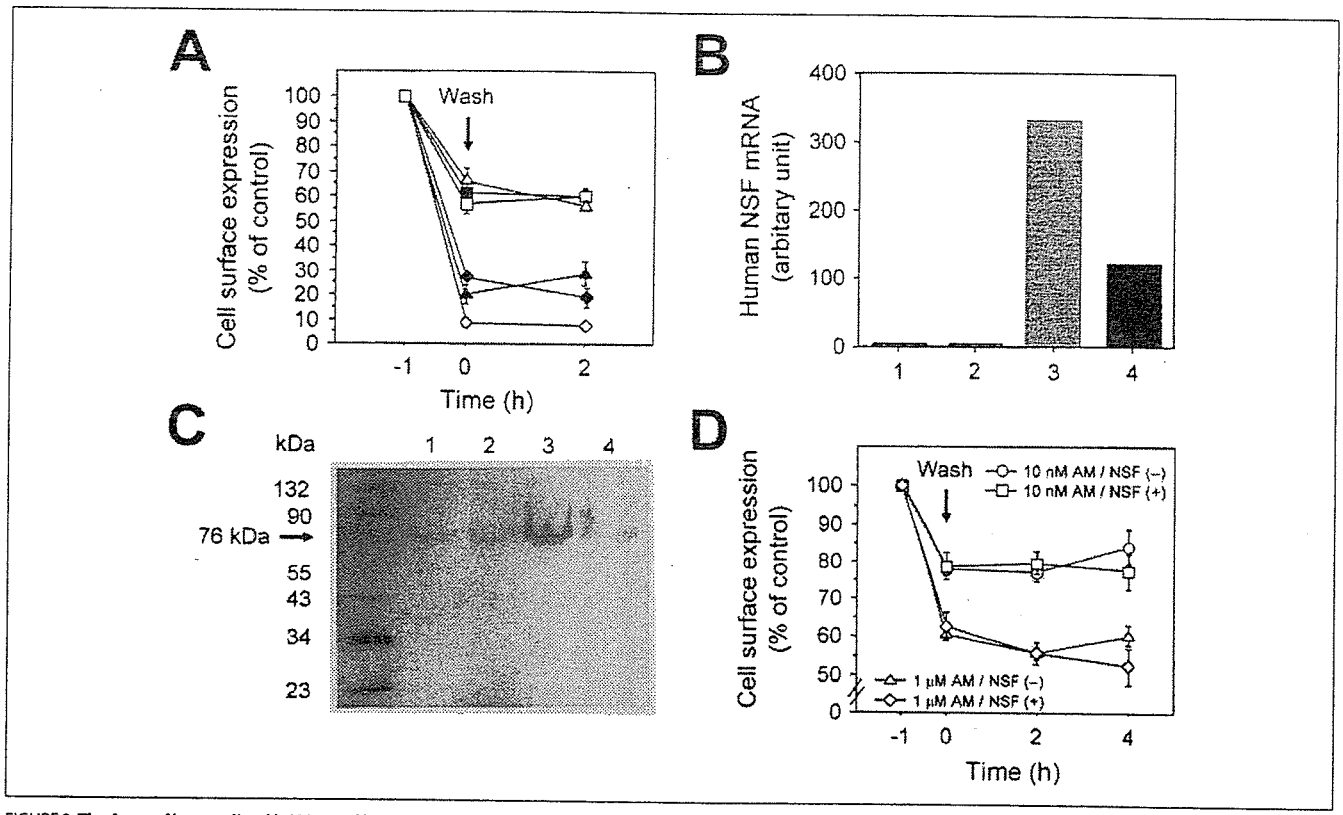

FIGURE 8. **The fates of internalized hCRLR and hRAMPs and their C-terminal deletion mutants.** *A*, FACS analysis of recycling of the internalized heterodimeric receptors. HEK-293 cells stably expressing CRLR-GFP were transiently transfected with each RAMP construct (*symbols* are the same as in Fig. 3*B*), after which they were incubated for 60 min with 1 μM αCGRP or AM plus 10 μg/ml cycloheximide and 10 μg/ml brefeldin A. The cells were then washed with prewarmed PBS and labeled with the indicated antibodies. Cell surface expression of each construct was estimated by flow cytometry. *Bars* represent means ± S.E. of three independent experiments. *B*, endogenous and transiently transfected hNSF mRNA levels. *1*, intact HEK-293 cells; *2*, HEK-293 cells stably expressing CRLR-GFP; *3*, NSF-transfected HEK-293 cells; *4*, NSF-transfected HEK-293 cells stably expressing CRLR-GFP. Expression of NSF mRNA was assessed using real time quantitative PCR with the appropriate primers and probes. Levels of NSF mRNA were normalized to that of GAPDH mRNA, which served as an internal control. *Bars* represent the average of two experiments. *C*, Western analysis of endogenous NSF and overexpressed NSF in HEK-293 cells. Equal aliquots of protein (20 μg) were subjected to 10% SDS gel electrophoresis. *Lane 1*, cells expressing empty vector (*Mock*); *lane 2*, cells stably expressing CRLR-GFP; *lane 3*, cells transiently expressing NSF; *lane 4*, cells expressing both CRLR-GFP and NSF. The blots shown are representative of three independent experiments. *D*, FACS analysis of the recycling of CRLR and RAMP3 in the presence and absence of NSF. CRLR-GFP-expressing cells were transiently transfected with VS-RAMP3 plus empty vector or NSF, after which they were incubated for 60 min with 10 nM or 1 μM AM plus 10 μg/ml cycloheximide and 10 μg/ml brefeldin A. The cells were then treated as described in *A*. Cell surface expression of each construct was estimated by flow cytometry. The *symbols* represent means ± S.E. of three independent experiments.

been no studies on the relation between the SK sequence and surface delivery of other GPCRs, but the LL sequence in the C-tail of the V_2 vasopressin receptor was found to be crucial for ER-to-Golgi transfer of that receptor, presumably by helping establish a correct and transport-competent folding state (36). Similarly, RAMPs appear to mediate transport of the CRLR from the ER to the Golgi, since CRLR was restricted to the ER in the absence of RAMPs (6). It therefore seems likely that the SK sequence in the RAMP2 C-tail, but not that in the RAMP3 C-tail, is essential for the escape of CRLR from the ER. The mechanism underlying the differential effect of the SK sequence on the cellular trafficking of these two AM receptors remains to be determined.

There have been two studies on the effects of CGRP in HEK-293 cells coexpressing hCRLR with a hRAMP1 C-tail deletion mutant (19, 32). One found that the C-tail deletion resulted in a 1-order of magnitude reduction in CGRP-stimulated cAMP formation, but no data on CGRP binding were shown (19). In that case, the 140th residue Gln, but not the SK sequence, most likely determined the affinity of CGRP for the receptor. The other study found no significant changes in CGRP binding or signaling (32). Similarly, we found that deleting the C-tail of RAMP1 had little effect on receptor signaling, as reflected by CGRP-evoked cAMP production, although the binding profile we obtained differed from that obtained in the earlier study (32). This absence of a significant change in the potency of CGRP may indicate that there was little change in the internalization of CRLR-GFP. In contrast to the αCGRP responses, ^{125}I-[Tyr^0]αCGRP binding to CRLR-GFP/Δ139-RAMP1 was much diminished. This discrepancy could be due in part to interference by the extra N-terminal tyrosine residue (Tyr^0). In any event, the contribution of the RAMP1 C-tail to CGRP potency is much smaller than that made by its extracellular domain (13, 17, 32, 34, 35).

Several earlier studies showed that internalized CRLR/RAMP heterodimers are trafficked to lysosomes for degradation (6, 10). It is now recognized that receptor ubiquitination is essential for proper trafficking to lysosomes (43). Indeed, our CRLR-GFP-transfected HEK-293 cells abundantly expressed endogenous ubiquitin, which attaches to lysine residues within the substrate proteins (data not shown). Nevertheless, truncation of RAMP C-tails that removed the Lys residues failed to promote recycling of CRLR-GFP. This raises the possibility that expression of intracellular proteins involved in mediating appropriate receptor recycling was inadequate in the HEK-293 cells used. NSF, like NHERF, is believed to enhance recycling of internalized receptors (44), and it was recently shown that NSF interacts with the PDZ motif of hRAMP3, enabling internalized AM_2 receptors to undergo slow recycling (18). Notably, although rat and mouse RAMP3 tails contain an RLL sequence instead of a PDZ motif, NSF also promoted recycling of CRLR/RAMP3 heterodimers

(18). In the present study, however, the cells abundantly expressed endogenous NSF, making it unlikely that poor expression of NSF underlies the trafficking of CRLR-GFP/RAMP3 to lysosomes without recycling. Even overexpression of NSF in these cells did not alter the AM-mediated trafficking of AM_2 receptors.

The rapid recycling pathway has been best studied and characterized for the β_2-AR, which has a PDZ motif in its C-tail (14, 15, 30) and which requires both NHERF and NSF for its recycling (30, 44). Indeed, among 59 representative seven-transmembrane segment GPCRs tested, NSF bound most strongly to the β_2-AR tail (44). However, a point mutation within the PDZ motif that disrupted the binding of NSF, but not that of NHERF, had no effect on β_2-AR recycling (30). In addition, the β_1-AR and cystic fibrosis transmembrane regulator each contain a C-terminal PDZ binding sequence (SKV and TRL, respectively) and undergo rapid recycling, despite their failure to bind NSF (30). Thus, NSF binding to GPCRs and RAMP3 is not required for recycling of proteins containing PDZ binding sequences.

In summary, our results indicate that the C-tails of hRAMP2 and -3 are involved in hCRLR surface delivery and internalization, respectively, and that the highly conserved SK sequence within their C-tails is a key determinant of the cellular behavior of the AM_1 and AM_2 receptors.

REFERENCES

1. Kitamura, K., Kangawa, K., Kawamoto, M., Ichiki, Y., Nakamura, S., Matsuo, H., and Eto, T. (1993) *Biochem. Biophys. Res. Commun.* **192,** 553–560
2. Eto, T. (2001) *Peptides* **22,** 1693–1711
3. Poyner, D. R., Sexton, P. M., Marshall, I., Smith, D. M., Quirion, R., Born. W., Muff, R., Fischer, J. A., and Foord, S. M. (2002) *Pharmacol. Rev.* **54,** 233–246
4. McLatchie, L. M., Fraser, N. J., Main, M. J., Wise, A., Brown, J., Thompson, N., Solari, R., Lee, M. G., and Foord, S. M. (1998) *Nature* **393,** 333–339
5. Sexton, P. M., Albiston, A., Morfis, M., and Tilakaratne, N. (2001) *Cell Signal.* **13,** 73–83
6. Hilairet, S., Belanger, C., Bertrand, J., Laperriere, A., Foord, S. M., and Bouvier, M. (2001) *J. Biol. Chem.* **276,** 42182–42190
7. Kuwasako, K., Cao, Y-N., Nagoshi, Y., Kitamura, K., and Eto, T. (2004) *Peptides* **25,** 2003–2012
8. Nagoshi, Y., Kuwasako, K., Ito, K., Uemura, T., Kato, J., Kitamura, K., and Eto, T. (2002) *Eur. J. Pharmacol.* **450,** 237–243
9. Muff, R., Born, W., and Fischer, J. A. (2003) *Hypertens. Res.* **26,** 3–8
10. Kuwasako, K., Shimekake, Y., Masuda, M., Nakahara, K., Yoshida, T., Kitaura, M., Kitamura, K., Eto, T., and Sakata, T. (2000) *J. Biol. Chem.* **275,** 29602–29609
11. Kuwasako, K., Kitamura, K., Ito, K., Uemura, T., Yanagita, Y., Kato, J., Sakata, T., and Eto, T. (2001) *J. Biol. Chem.* **276,** 49459–49465
12. Kuwasako, K., Kitamura, K., Onitsuka, H., Uemura, T., Nagoshi, Y., Kato, J., and Eto, T. (2002) *FEBS Lett.* **519,** 113–116
13. Kuwasako, K., Kitamura, K., Nagoshi, Y., Cao Y-N., and Eto, T. (2003) *J. Biol. Chem.* **278,** 22623–22630
14. Koenig, J. A., and Edwardson, J. M. (1997) *Trends. Pharmacol. Sci.* **18,** 276–287
15. Krupnick, J. G., and Benovic, J. L. (1998) *Annu. Rev. Pharmacol. Toxicol.* **38,** 289–319
16. Ferguson, S. S. G. (2001) *Pharmacol. Rev.* **53,** 1–24
17. Hay, D. L., Poyner, D. R., and Sexton, P. M. (2006) *Pharmacol. Ther.* **109,** 173–197
18. Bomberger, J. M., Parameswaran, N., Hall, C. S., Aiyar, N., and Spielman, W. S. (2005) *J. Biol. Chem.* **280,** 9297–9307
19. Steiner, S., Muff, R., Gujer, R., Fischer, J. A., and Born, W. (2002) *Biochemistry* **41,** 11398–11404
20. Hicke, L., and Riezman, H. (1996) *Cell* **84,** 277–287
21. Roth, A. F., and Davis, N. G. (1996) *J. Cell Biol.* **134,** 661–674
22. Martin, N. P., Lefkowitz, R. J., and Shenoy, S. K. (2003) *J. Biol. Chem.* **278,** 45954–45959
23. Shenoy, S. K., and Lefkowitz, R. J. (2003) *J. Biol. Chem.* **278,** 14498–14506
24. Kuwasako, K., Cao, Y-N., Nagoshi, Y., Tsuruda, T., Kitamura, K., and Eto, T. (2004) *Mol. Pharmacol.* **65,** 207–213
25. Aiyar, N., Rand, K., Elshourbagy, N. A., Zeng, Z., Adamou, J. E., Bergsma, D. J., and Li, Y. (1996) *J. Biol. Chem.* **271,** 11325–11329
26. Guon, X.-M., Kobilka, T. S., and Kobilka, B. K. (1992) *J. Biol. Chem.* **267,** 21995–21998
27. Nagoshi, Y., Kuwasako, K., Cao, Y-N., Kitamura, K., and Eto, T. (2004) *Biochem. Biophys. Res. Commun.* **314,** 1057–1063
28. Cao, Y-N., Kuwasako, K., Kato, J., Yanagita, T., Tsuruda, T., Kawano, J., Nagoshi, Y., Chen, A. F., Wada, A., Suganuma, T., Eto, T., and Kitamura, K. (2005) *Biochem. Biophys. Res. Commun.* **332,** 866–872
29. Xu, J., and Tse, F. W. (1999) *J. Biol. Chem.* **274,** 19095–19102
30. Gage, R. M., Matveeva, E. A., Whiteheart, S. W., von Zastrow, M. (2005) *J. Biol. Chem.* **280,** 3305–3313
31. McDonald, P. H., Cote, N. L., Lin, F-T., Premont, R. T., Pitcher, J. A., and Lefkowitz, R. J. (1999) *J. Biol. Chem.* **274,** 10677–10680
32. Fitzsimmons, T. J., Zhao, X., and Wank, S. A. (2003) *J. Biol. Chem.* **278,** 14313–14320
33. Bomberger, J. M., Spielman, W. S., Hall, C. S., Weinman, E. J., and Parameswaran, N. (2005) *J. Biol. Chem.* **280,** 23926–23935
34. Fraser, N. J., Wise, A., Brown, J., McLatchie, L. M., Main, M. J., and Foord, S. M. (1999) *Mol. Pharmacol.* **55,** 1054–1059
35. Hilairet, S., Foord, S. M., Marshall, F. H., and Bouvier, M. (2001) *J. Biol. Chem.* **276,** 29575–29581
36. Schulein, R., Hermosilla, R., Oksche, A., Dehe, M., Wiesner, B., Krause, G., and Rosenthal, W. (1998) *Mol. Pharmacol.* **54,** 525–535
37. Nakamura, K., and Ascoli, M. (1999) *Mol. Pharmacol.* **56,** 728–736
38. Dietrich, J., Kastrup, J., Nielsen, B. L., Odum, N., and Geisler, C. (1997) *J. Cell Biol.* **138,** 271–281
39. Kirchhausen, T., Bonifacino, J. S., and Riezman, H. (1997) *Curr. Opin. Cell Biol.* **9,** 488–495
40. Rapoport, I., Chen, Y-C., Cupers, P., Shoelson, S. E., and Kirchhausen, T. (1998) *EMBO J.* **17,** 2148–2155
41. Tamai, K., Semenov, M., Kato, Y., Spokony, R., Liu, C., Katsuyama, Y., Hess, F., Saint-Jeannet, J. P., and He, X. (2000) *Nature* **407,** 530–535
42. Lazar, C. S., Cresson, C. M., Lauffenburger, D. A., and Gill, G. N. (2004) *Mol. Biol. Cell* **15,** 5470–5480
43. Wojcikiewicz, R. J. H. (2004) *Trends Pharmacol. Sci.* **25,** 35–41
44. Heydorn, A., Sondergaard, B. P., Ersboll, B., Holst, B., Nielsen, F. C., Haft, C. R., Whistler, J., and Schwartz, T. W. (2004) *J. Biol. Chem.* **279,** 54291–54303

Brief Review

Adrenomedullin
A Protective Factor for Blood Vessels

Johji Kato, Toshihiro Tsuruda, Toshihiro Kita, Kazuo Kitamura, Tanenao Eto

Abstract—Adrenomedullin (AM) is a vasodilator peptide having a wide range of biological actions such as reduction of oxidative stress and inhibition of endothelial cell apoptosis. The AM gene is expressed in vascular walls, and AM was found to be secreted from cultured vascular endothelial cells, smooth muscle cells, and adventitial fibroblasts. Plasma AM levels in patients with arteriosclerotic vascular diseases are elevated in possible association with the severity of the disease. When administered over a relatively short period, AM dilates blood vessels via an endothelium-dependent or independent mechanism. Experiments in vitro have shown that AM exerts multiple actions on cultured vascular cells, which are mostly protective or inhibitory against vascular damage and progression of arteriosclerosis. Either prolonged infusion or overexpression of AM suppressed intimal thickening, fatty streak formation, and perivascular hyperplasia in rodent models for vascular remodeling or atherosclerosis. Intimal thickening induced by periarterial cuff was more severe in AM gene-knockout mice than their littermates, suggesting a protective role for endogenous AM. Moreover, AM has recently been suggested to possess angiogenetic properties. Collectively, a body of evidence suggests that AM participates in the mechanism against progression of vascular damage and remodeling, thereby alleviating the ischemia of tissues and organs. (***Arterioscler Thromb Vasc Biol.* 2005;25:2480-2487.**)

Key Words: adrenomedullin ■ vasodilatation ■ endothelium ■ smooth muscle cell ■ arteriosclerosis

Cardiovascular diseases secondary to arteriosclerosis of blood vessels are currently among the leading causes of death in developed countries. A number of factors, both humoral and mechanical, have been shown to modulate vascular function in humans as well as in experimental animals.[1] Blood vessel dysfunction resulting from an imbalance of those factors accelerates the process of vascular remodeling and atherosclerosis.[1] Vasoconstrictors including angiotensin II and endothelins not always but mostly act as proatherogenic factors, whereas vasodilators, either peptides or non-peptides, such as natriuretic peptides, nitric oxide (NO), and prostaglandin (PG) I_2, have antiatherogenic properties.[1] In 1993, a new vasodilator peptide, adrenomedullin (AM), was isolated from the tissue extract of a human pheochromocytoma by monitoring cAMP levels in rat platelets.[2] Substantial levels of the AM peptide and gene expression were detected in the cardiovascular tissues including blood vessels. As listed in the Table, AM was found to exert a wide range of biological actions related to vascular functions in cultured cells, with which observations in vivo have been mostly accordant. Ever since the discovery of AM, efforts have been made to clarify the role of this bioactive peptide in blood vessels and a substantial amount of basic and clinical data has been accumulated. In this review, after summarizing the biochemical and pharmacological features of AM, we discuss its role in blood vessels, which is assumed to be protective, or inhibitory against the progression of vascular damage and remodeling.

Biochemistry of AM

Human AM is a 52-aa peptide with a ring structure formed by a disulfide bond and amidated tyrosine at the C terminus (Figure 1), both essential for binding to receptors and biological activity.[2–4] Based on sequence homology, AM is thought to belong to the calcitonin gene–related peptide (CGRP) superfamily.[2–4] Cloning of the cDNA encoding AM revealed the AM precursor peptide preproAM to comprise 185 amino acids, with the C terminus followed by a pair of basic amino acids, Arg-Arg, a typical processing signal (Figure 2).[5] In addition to AM, preproAM was found to contain another bioactive peptide, proadrenomedullin N-terminal 20 peptide (PAMP), in the N-terminal portion.[5] PAMP lowered blood pressure when injected intravenously, but its action is weaker than that of AM and there is currently little information available as to the role of PAMP in the vasculature.[3,4] In a sequence analysis of the genomic DNA for human preproAM, AM was found to be encoded in the fourth exon and PAMP in the second and third exons (Figure 2).[6] When processed from preproAM, AM-Gly, an intermediate form (iAM), is produced, and then iAM is converted by the amidation enzyme to the mature form of AM (mAM) having an amide structure at the C terminus.[7] The mature form of PAMP is thought to be produced by a similar process (Figure 2).

Original received May 17, 2005; final version accepted July 11, 2005.
From the First Department of Internal Medicine, Miyazaki Medical College, University of Miyazaki, Japan
Correspondence to Johji Kato, MD, PhD, First Department of Internal Medicine, Miyazaki Medical College, University of Miyazaki, 5200 Kihara, Kiyotake, Miyazaki 889-1692, Japan. E-mail jkjpn@med.miyazaki-u.ac.jp

Arterioscler Thromb Vasc Biol. is available at http://www.atvbaha.org DOI: 10.1161/01.ATV.0000184759.91369.f8

Biological Actions of AM on Cultured Vascular Cells

Cell Type	Observed Effects	Reference No.
Endothelial cells	Elevation of cAMP level	30, 32, 65
	Intracellular Ca^{2+} mobilization	65
	Stimulation of NO production	65
	Stimulation of proliferation and migration	67
	Inhibition of apoptosis	61, 62, 66
Smooth muscle cells	Elevation of cAMP level	21, 34
	Inhibition or stimulation of proliferation	68, 69
	Inhibition of migration	34, 70
	Reduction of oxidative stress	71
Adventitial fibroblasts	Elevation of cAMP level	72
	Inhibition of proliferation	39
	Augmentation of metalloproteinase-2 action	72

In an effort to isolate unknown bioactive peptides having sequence homology with AM, another member belonging to the CGRP superfamily was recently discovered independently by two groups and named intermedin/AM-2.[8,9] Human intermedin/AM-2 consists of 47 amino acid residues with an intramolecular ring structure formed by a disulfide bond and amidated tyrosine at the C terminus, showing structural homology with AM.[8,9] Intermedin/AM-2 was shown to shear the receptors with AM by cultured cells,[8] and in accord with this, it exerted vasodilator actions similar to AM ex vivo.[10] However, data on the biochemical and pharmacological features of this novel peptide are currently very limited, and further characterization, such as the tissue distribution and effects on vascular cells, is necessary to discuss its role in blood vessels.

Vasodilator Action of AM

The biological feature of AM initially characterized was a potent, long-lasting, blood pressure–lowering effect with reduced peripheral resistance after intravenous bolus injection or infusion in a relatively short period of time.[2,11,12] The hypotensive effect of AM observed in those studies was shown to be largely secondary to direct vasodilatation,[11,12] which was further demonstrated by ex vivo studies with isolated rat aorta and with perfused rat mesenteric artery.[13,14]

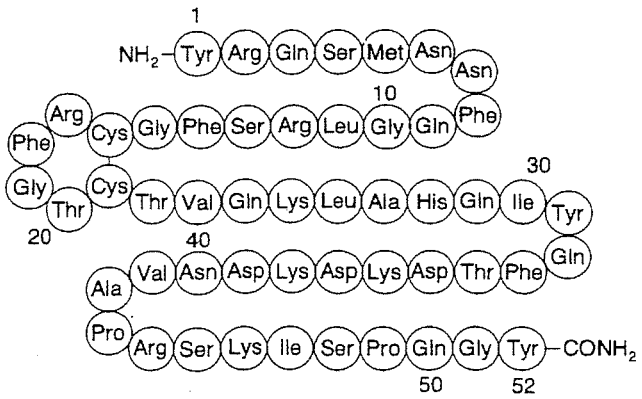

Figure 1. Amino-acid sequence of human AM.

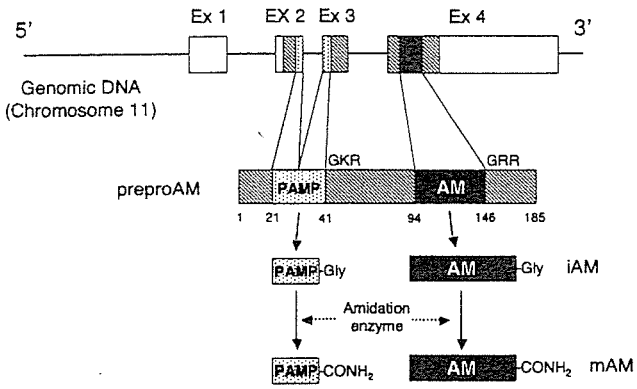

Figure 2. Schematic representations of the AM gene and of the processing of AM and PAMP from preproAM. Ex indicates exon; PAMP, proadrenomedullin N-terminal 20 peptide; iAM and iPAMP, intermediate forms of AM and PAMP, respectively; mAM and mPAMP, mature forms of AM and PAMP, respectively.

The mechanisms by which AM dilates blood vessels are not completely understood; however, based on the numerous articles published to date, it is clear that AM directly dilates blood vessels of the systemic and pulmonary circulation in an endothelium-dependent or independent manner.[14–23]

AM has been shown to exert an endothelium-dependent vasodilatation via the NO-cyclic GMP (cGMP) pathway in rat aorta, in renal or hindquarter vascular bed of rats, and in canine kidneys.[14–17] In a further analysis of the mechanism, AM dilated rat aorta by activating phosphatidylinositol 3-kinase (PI3K) and Akt via the Ca^{2+}/calmodulin-dependent pathway, which leads to increased production of NO through phosphorylation of endothelial NO synthase.[18] On the other hand, endothelium-independent vasodilatation by AM has also been shown ex vivo in experiments with dog arteries or porcine coronary artery.[19,20] The mechanisms so far proposed for endothelium-independent vasodilatation are an increase in the intracellular cyclic AMP (cAMP) level, a decrease in the Ca^{2+} concentration, and the activation of K^+ channels in vascular smooth muscle cells (SMCs).[21–23]

In humans, similarly to animals, intravenous infusion of AM lowered systemic and pulmonary vascular resistance, reducing blood pressure and increasing heart rate.[24] AM-induced forearm arterial vasodilatation in healthy human subjects was attenuated by N-monomethyl-L-arginine (L-NMMA).[25] In human coronary arterioles, vasodilatation induced by AM ex vivo was found to be dependent on the generation of NO and the activation of K^+ channels, but not on guanylate or adenylate cyclase.[26] A difference between species was also observed regarding the mechanisms. For example, pulmonary vasodilator responses were reduced by N-nitro-L-arginine methyl ester (L-NAME) in rats, but not in cats.[27] Currently, there is little data available on the vasodilator effect on veins, whereas Barder et al reported that vasodilatation of femoral veins in canines was endothelium-dependent, but independent of cAMP and cGMP.[28] Thus, the mechanism by which AM achieves direct vasodilatation appears to differ depending on species, the size of blood vessels, or regions where the vessels are isolated.